Heparan sulfate dependent binding of plasmatic von Willebrand factor to blood circulating melanoma cells attenuates metastasis

Yuanyuan Wang [a,b,1], Xiaobo Liu [a,1], Tobias Obser [a], Alexander T. Bauer [a], Martin Heyes [c], Sarah Starzonek [d], Mina Zulal [a], Karena Opitz [a], Leonie Ott [e], Sabine Riethdorf [e], Tobias Lange [d], Klaus Pantel [e], Gerd Bendas [c], Stefan W. Schneider [a], Marion Kusche-Gullberg [f] and Christian Gorzelanny [a]

***a* - Department of Dermatology and Venereology, Experimental Dermatology,** *University Medical Center Hamburg-Eppendorf, Martinistr. 52, Hamburg 20246, Germany*
***b* - Department of Dermatology, Medical Faculty Mannheim,** *University of Heidelberg, Mannheim 68167, Germany*
***c* - Department of Pharmacy,** *Rheinische Friedrich Wilhelms University Bonn, Bonn 53113, Germany*
***d* - Institute of Anatomy and Experimental Morphology,** *University Medical Center Hamburg-Eppendorf, Hamburg 20246, Germany*
***e* - Department of Tumor Biology,** *University Medical Center Hamburg-Eppendorf, Hamburg 20246, Germany*
***f* - Department of Biomedicine,** *University of Bergen, Bergen 5009, Norway*

Corresponding author. ***c.gorzelanny@uke.de.***
https://*doi.org/10.1016/j.matbio.2022.06.002*

Abstract

Heparan sulfate (HS), a highly negatively charged glycosaminoglycan, is ubiquitously present in all tissues and also exposed on the surface of mammalian cells. A plethora of molecules such as growth factors, cytokines or coagulation factors bear HS binding sites. Accordingly, HS controls the communication of cells with their environment and therefore numerous physiological and pathophysiological processes such as cell adhesion, migration, and cancer cell metastasis. In the present work, we found that HS exposed by blood circulating melanoma cells recruited considerable amounts of plasmatic von Willebrand factor (vWF) to the cellular surface. Analyses assisted by super-resolution microscopy indicated that HS and vWF formed a tight molecular complex. Enzymatic removal of HS or genetic engineering of the HS biosynthesis showed that a reduced length of the HS chains or complete lack of HS was associated with significantly reduced vWF encapsulation. In microfluidic experiments, mimicking a tumor-activated vascular system, we found that vWF-HS complexes prevented vascular adhesion. In line with this, single molecular force spectroscopy suggested that the vWF-HS complex promoted the repulsion of circulating cancer cells from the blood vessel wall to counteract metastasis. Experiments in wild type and vWF knockout mice confirmed that the HS-vWF complex at the melanoma cell surface attenuated hematogenous metastasis, whereas melanoma cells lacking HS evade the anti-metastatic recognition by vWF. Analysis of tissue samples obtained from melanoma patients validated that metastatic melanoma cells produce less HS. Transcriptome data further suggest that attenuated expression of HS-related genes correlate with metastases and reduced patients' survival. In conclusion, we showed that HS-mediated binding of plasmatic vWF to the cellular surface can reduce the hematogenous spread of melanoma. Cancer cells with low HS levels evade vWF recognition and are thus prone to form metastases. Therefore, therapeutic expansion of the cancer cell exposed HS may prevent tumor progression.

Introduction

Heparan sulfate (HS) belongs to the family of glycosaminoglycans and covers every mammalian cell. It is part of the glycocalyx and anchored to the cell surface by proteoglycans namely syndecans (SDC) and glypicans. The mammalian syndecan family has four members (SDC1-4) and the number of HS chains they expose ranges from two to four. The mammalian glypican family consists of six members exposing one to three HS chains [1,2]. The biosynthesis and postsynthesis processing of HS is a complex process that involves the action of various enzymes. After synthesis of the linker region at the protein backbone, the HS chain is elongated by the action of the two glycosyltransferases exostosin 1 (EXT1) and EXT2. Subsequently, the HS chain is further sulfated by sulfotransferases producing a strongly negatively charged polymer with a length of hundreds of nanometers [3]. Previous studies document that the malignant behavior of cancer cells was strongly related to an aberrant synthesis and expression of HS [4,5]. In addition, enhanced degradation of HS by heparanase (HPSE) was linked to metastasis and reduced patients' survival [6,7]. We have recently shown that melanoma cells produce an altered HS and that approximately 40% of all melanoma patients suffer from genetic alterations within the biosynthesis machinery of HS [8]. HS forms, in concert with other glycocalyx components, a gel-like layer that controls the interaction of the cell with its environment by regulating e.g. the perception of cytokines [9,10], the function of integrins [11,12], and the activity of coagulation factors [13]. Accordingly, we have previously shown that the HS of endothelial cells anchors the procoagulant vWF to the vascular wall [14].

VWF, one of the largest multimeric glycoproteins, bears binding sites for many adhesion molecules such as collagens or $\alpha_v\beta_3$ integrins [15]. In the past, the physiological function of vWF was considered to be the trapping of blood flowing platelets at sites of vascular injury. However, vWF accomplished several tasks beyond hemostasis [16]. Previous studies measured increased levels of plasmatic vWF in cancer patients [17–22]. In various tumor entities, the blood vWF concentration increases proportionally with the tumor stage and in correlation with the systemic spread of tumor cells [23]. However, the potential role of vWF in malignancy is controversial and acting molecular mechanisms remained to be clarified [24–27]. Because HS has the power to regulate the interaction of cancer cells with their environment, we investigated the impact of melanoma cell exposed HS on vWF binding and we clarified to which extend the interaction between HS and vWF affects cell adhesion and metastasis.

Metastasis is a common complication in late stage melanoma patients and strongly associated with a reduced survival. Melanoma cells were prone to metastasize into distant organs such as the lung or the brain [28]. After intravasation into the vascular system, cancer cells are instantaneously exposed to harsh conditions comprising mechanical forces, the immune and coagulation system. Escape from this detrimental environment defines the ability of the circulating tumor cells (CTCs) to extravasate and to from metastatic foci [29]. Depending on their origin and their genetic repertoire, cancer cells developed different evasion strategies to prevent elimination by the immune or coagulation system and to facilitate the adhesion to the blood vessel wall and the transmigration into the adjacent tissue [30]. Previous studies investigated the interaction of blood flowing cancer cells with platelets, leucocytes and endothelial cells [31]. However, research investigating the interaction between blood circulating cancer cells and plasma proteins are rare and the potential molecular interplay between the HS of blood circulating cancer cells and soluble interaction partners such as plasmatic vWF is unknown.

In the present work, we characterized the glycocalyx and in particular the extent of HS, which is exposed by human and murine melanoma cells. Moreover, we studied the impact of HS on vWF binding and whether the HS mediated binding of vWF to blood flowing cancer cells affected their ability to adhere to the vascular endothelium and thus to form metastasis.

Results

Plasmatic vWF encircles blood flowing melanoma cells

To prove that blood flowing melanoma cells can interact with plasmatic vWF, we spiked human whole blood with MV3 cells. Fig. 1A, B shows that MV3 cells accumulated vWF at their surface, whereas leucocytes remained vWF negative, indicating a highly specificity binding of the plasmatic vWF to the melanoma cell surface. Because our previous work suggest that cell surface attached HS is a relevant binding partner for vWF [14], we investigated the impact of melanoma cell exposed HS on vWF binding. Next to MV3, we selected two additional melanoma cell lines (IGR37 and B16F10) that expose different levels of HS (Fig. 1C, D). Fig. 1 E, F shows that the accumulation of vWF at the cellular surface was in direct proportion to the HS levels.

Terraube et al. proposed that integrin $\alpha_v\beta_3$ mediates the interaction between vWF and melanoma cells [26]. It is worth mentioning, that in this previous study, the attachment of melanoma cells to vWF coated surfaces was measured, whereas we aim to understand the interaction between flowing

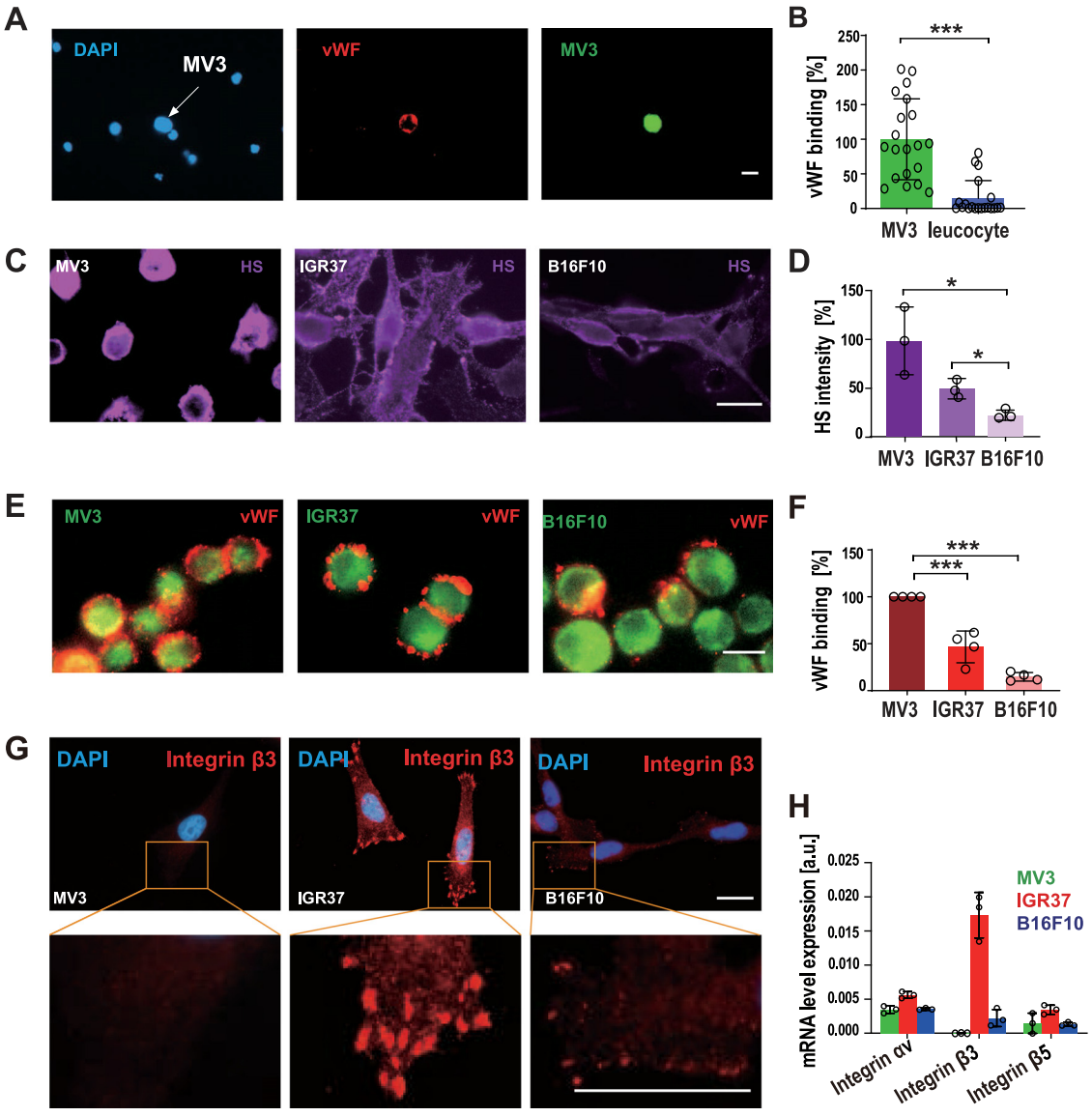

Fig. 1. Different melanoma cells have distinct vWF binding capacities. (A) Whole human blood spiked with MV3 cells. MV3 cells (green) but not leucocytes (blue) interact with plasmatic vWF (red). (B) Quantification of vWF binding to MV3 cells and leucocytes (n = 20). (C) Expression of HS by the melanoma cell lines MV3, IGR37 and B16F10 was measured by fluorescence microscopy and (D) flow cytometry (n = 3). (E) Binding of vWF to MV3, IGR37 and B16F10 cells was detected by fluorescence microscopy. (F) Quantification of vWF binding to MV3, IGR37 and B16F10 by on-cell ELISA (n = 4). (G) Protein levels of Integrin β_3 expression in the three selected melanoma cell lines using fluorescence microscopy. (H) Transcription of integrin α_v, β_3 and β_5 in the three selected melanoma cell lines was measured by qPCR (n = 3). Scale bars = 10 μm. Data are presented as the mean ± SD, $^*P < 0.05$, $^{**}P < 0.005$, $^{***}P < 0.0005$.

melanoma cells and soluble vWF. To clarify the role of integrins for the accumulation of soluble vWF, we measured the protein levels of β_3 and the mRNA expression of $\alpha_v\beta_3$ and β_5 in the three selected melanoma cell lines (Fig. 1G,H). Although all three cell lines expressed $\alpha_v\beta_3$ integrins, the expression levels did not correlate with the capability of the cells to bind plasmatic vWF.

Binding of vWF depends on HS

To better understand the molecular basis of the vWF binding to melanoma cells, we investigated the ability of different recombinant vWF mutants to interact with MV3 cells. We included vWF lacking the A1 domain and we explored vWF lacking the RGD-motif, the binding site for $\alpha_v\beta_3$ integrins (Fig. 2A).

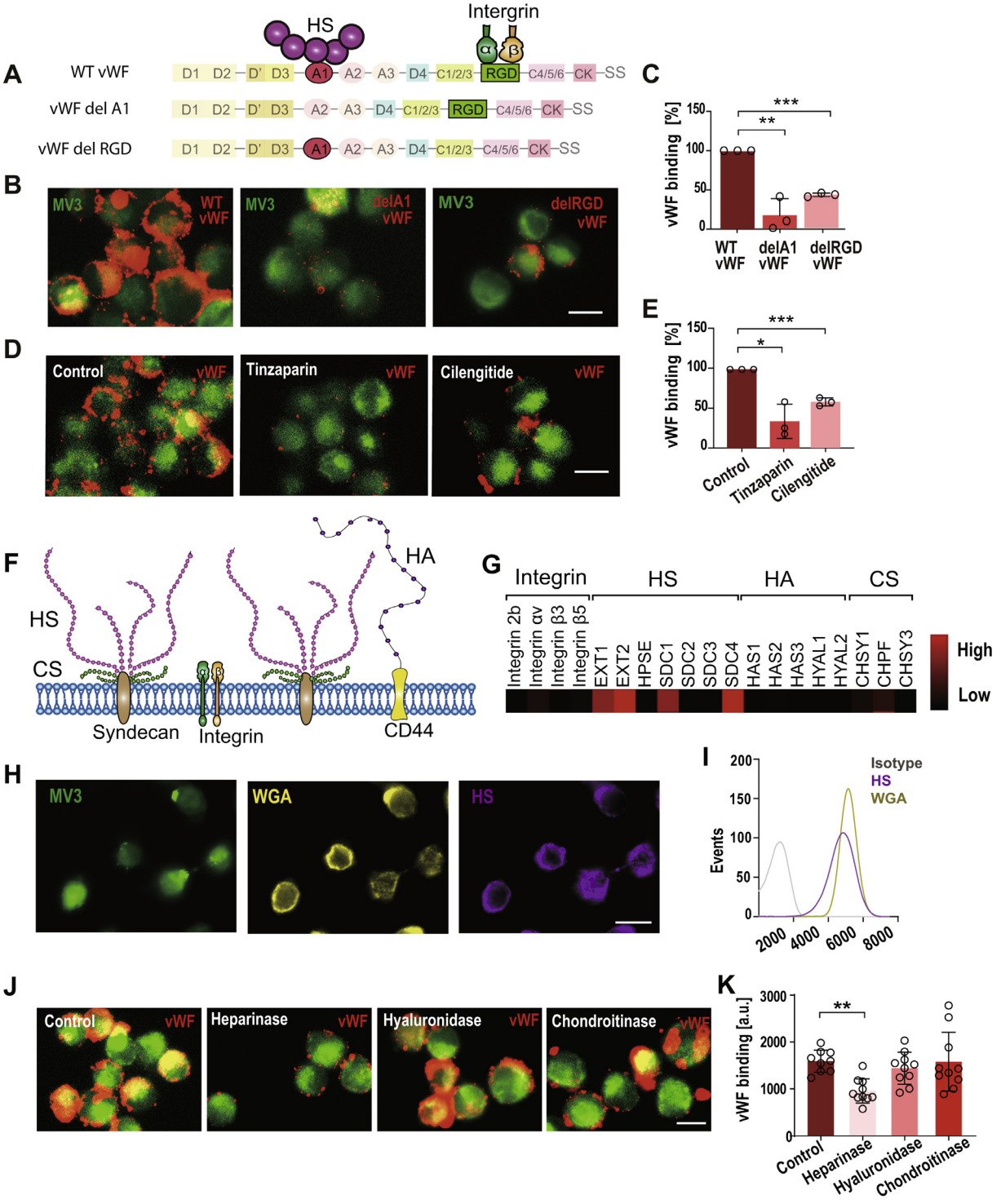

Fig. 2. Binding of vWF to melanoma cells depends on HS. (A) Schematic drawing of wild type (WT) vWF, vWF lacking the A1 domain, and vWF lacking the RGD-motif. RGD motif is the binding site for $\alpha_v\beta_3$ and β_5 integrins, A1 domain is a potential binding site for HS. (B) Lack of the A1 domain or the RGD motif attenuated the binding of vWF to MV3 cells. (C) Quantification of vWF binding by on-cell ELISA (n = 3). (D) Cilengtide and Tinzaparin blocked the binding of vWF to MV3 cells. Tinzaparin binds competitively to A1 domains. Cilengitide is an inhibitor of $\alpha_v\beta_3$ integrin. (E) Quantification of vWF binding by on-cell ELISA (n = 3). (F) Schematic drawing of cell surface integrins and glycocalyx components. HS and chondroitin sulfate (CS) chains are covalently attached to syndecans. Hyaluronic acid (HA) is non-covalently linked to CD44 (G) Expression levels of integrins and enzymes involved in glycocalyx synthesis in MV3 cells measured by qPCR.

Lack of the A1 HS binding domain reduced the binding of vWF strongly (Fig. 2B, C). Also lack of the RGD-motif attenuated vWF binding, but the effect was less pronounced. In further experiments, we applied tinzaparin and cilengitide to block the interaction between vWF and melanoma cells. Tinzaparin is a low-molecular weight heparin blocking the A1 domain of vWF. Cilengitide mimics the RGD-motif and is therefore a potent inhibitor of $\alpha_v\beta_3$ integrins [32]. In agreement to our experiments with the vWF mutants, we confirmed that the inhibition of the A1 domain interfered stronger with the vWF accumulation than the blockage of integrins (Fig. 2D, E). Taken together our data suggest that the main driver of the interaction between melanoma cells and vWF is HS and the A1 domain of vWF.

Although our data suggest that HS is involved in the binding of vWF to melanoma cells, we cannot exclude that other polyanionic molecules at the cellular surface such hyaluronic acid (HA) or chondroitin sulfate (CS) contribute to the binding (Fig. 2F). Therefore, we measured the transcriptional expression of proteins involved in the biosynthesis and presentation of HS, HA and CS in MV3 cells (Fig. 2G). High levels of EXT1 and EXT2 suggest a strong abundance of HS. In contrast, the probed mRNAs of enzymes, which are related to the production of HA and CS were only weakly expressed. To further underpin that HS is the most dominant glycan on the melanoma cell surface, we co-stained MV3 cells with wheat germ agglutinin (WGA) and with a specific antibody directed against HS (10E4). In contrast to the HS-directed antibody, WGA detects HS, HA, CS and N-linked glycans through the recognition of N-acetyl-glucosamine. Fluorescence microscopy of MV3 cells revealed a strong co-localisation of the WGA and HS-related fluorescence (Fig. 2H) and flow cytometry indicated a comparable signal intensity of both stainings (Fig. 2I). To further show that HS is crucially involved in the accumulation of plasmatic vWF at the melanoma cell surface, we treated MV3 cells with heparinase to remove HS, with hyaluronidase to remove HA and with chondroitinase to remove CS (Fig. 2J). Our data shown in Fig. 2K indicate that HS is the most prominent binding partner of vWF on the surface of melanoma cells.

Genetic depletion of EXT1 abrogated HS biosynthesis in melanoma cells

To study the biological impact of the HS-vWF interaction on tumor metastasis we aimed to disrupt the HS biosynthesis in melanoma cells by genetic depletion of EXT1 [33]. EXT1 in concert with EXT2 are crucial for the synthesis of HS (S-Fig. 1A). We used shRNA to attenuate the expression of EXT1 in MV3 cells (MV3-shEXT1) (S-Fig. 1B). In murine B16F10 cells, we targeted *Ext1* by CRISPR/Cas9 ($B16F10^{Ext1-/-}$) (S-Fig. 1C). Previously, it was shown that the expression level of EXT1 and EXT2 is potentially connected to the amount of glucosaminyl N-deacetylase/N-sulfotransferase (NDST1) within the cell [34]. NDST1 acts downstream of the EXT1/EXT2 complex and introduces N-sulfate groups to the HS chain. To exclude that the genetic manipulation of EXT1 influence the expression of NDST1 and thus HS sulfation, we measured the expression level of NDST1 by qPCR. S-Fig. 1D shows that upon genetic manipulation of EXT1, NDST1 was not affected. This is also in line with the work of Busse et al. showing that down regulation of EXT1 did not strongly affect the distribution and amounts of N-sulfation [33].

Reduced HS exposure of engineered MV3 and B16F10 cells was characterized by immunofluorescence staining and flow cytometry (S-Fig. 2A−F). In comparison to the control cells, MV3 shEXT1 cells exposed 78 ± 6.8% less HS on their surface (S-Fig. 2C). CRISPR/Cas9 edited B16F10 cells were completely deficient in HS (S-Fig. 2F). To exclude that the reduced HS exposure was also related to the up-regulation of HPSE, we measured its mRNA expression by qPCR. S-Fig. 2G, H shows that manipulation of EXT1 expression in B16F10 and MV3 cells had no relevant impact on the expression of HPSE.

To obtain a more profound characterization of our cells, we isolated the proteoglycan-exposed carbohydrates. The molecular weight of the isolated HS and CS chains, which have been metabolically labeled by ^{35}S radioisotopes was studied by gel chromatography (S-Fig. 2I−N). MV3 shCTL cells expose HS with molecular weights between 43 and 210 kDa. MV3 shEXT1 cells produced shorter HS chains with molecular weights between 30 and 43 kDa (S-Fig. 2J). The molecular weight of HS produced by B16F10 cells was about 43 kDa, while $B16F10^{Ext1-/-}$ cells produced no HS (S-Fig. 2M). The molecular weight of CS remained almost unaffected in the genetically engineering cells (S-Fig. 2K,N). We used stimulated emission depletion (STED) microscopy to measure the proteoglycan density at the surface of the melanoma cells (Fig. 3A−D). Of note, lack of EXT1 reduced the proteoglycan size,

Heparanase (HPSE), Hyaluronan Synthase (HAS), Hyaluronidase (HYAL), Chondroitin sulfate synthase (CHSY), Chondroitin sulfate synthase 2 (CHPF). (H) Co-staining of HS and wheat germ agglutinin (WGA) on the surface of MV3 cells was visualized by fluorescence microscopy. WGA detects HS, HA, CS and N-linked glycans. (I) HS and WGA co-staining was measured by flow cytometry. (J) vWF binding of MV3 cells after enzymatic degradation of HS (heparinase), HA (hyaluronidase) and CS (chondroitinase). (K) Quantification of vWF binding measured by fluorescence microscopy (n = 10). Scale bars = 10 μm. Data are presented as the mean ± SD, $^*P < 0.05$, $^{**}P < 0.005$, $^{***}P < 0.0005$.

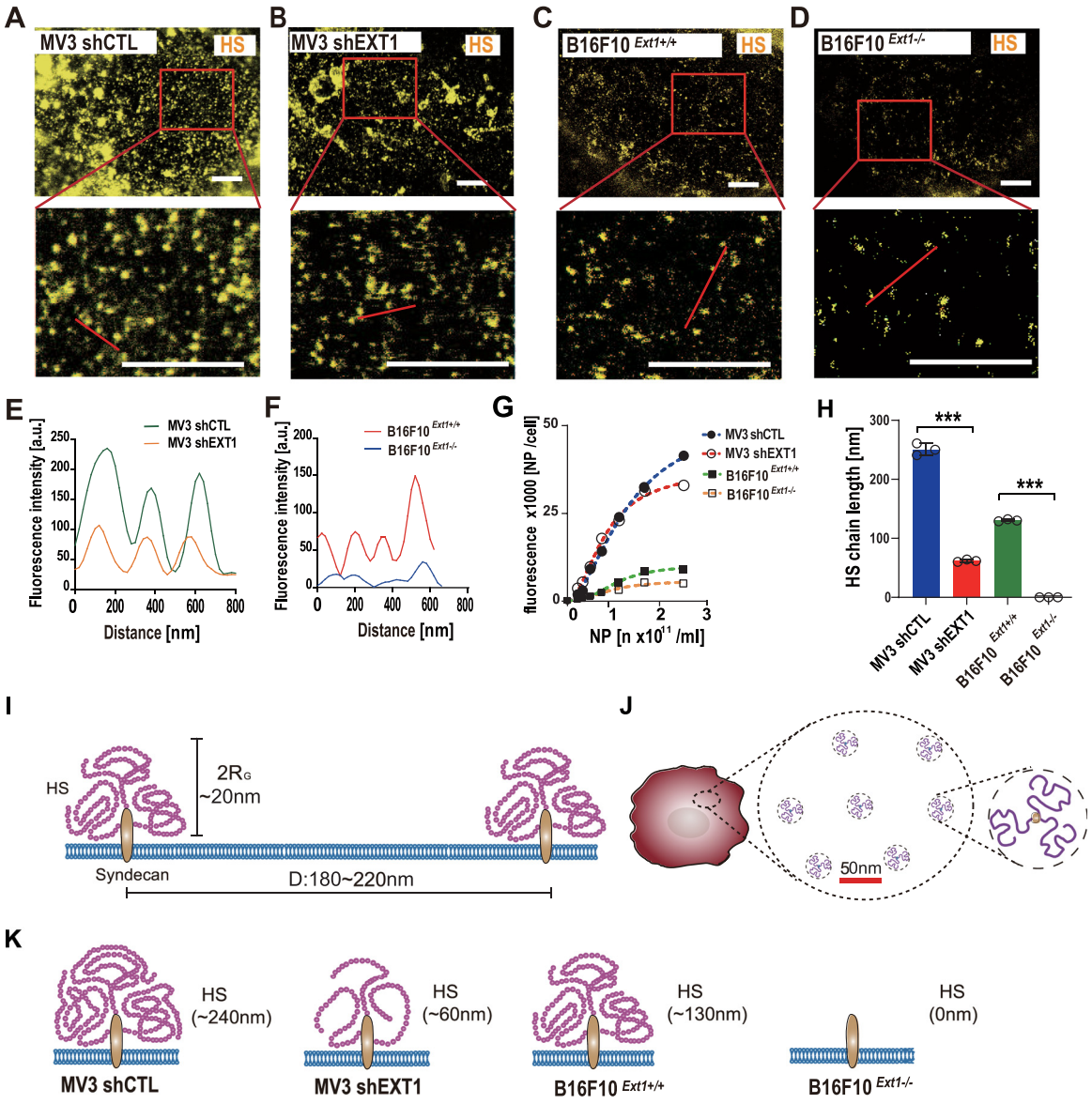

Fig. 3. Characterization of the melanoma cell glycocalyx. (A–D) Stimulated Emission Depletion (STED) microscopy showed nanometric cell surface proteoglycan distribution. Scale bars = 2 μm. (E,F) Distance of proteoglycans on the surface of MV3 and B16F10 cells was measured on STED images. (G) Dose-dependent nanoparticle (NP) binding to MV3 and B16F10 cells. (H) HS chain length determined on the basis of NP titration. ($n = 3$) (I) Side view of cell surface exposed HS chains. The thickness of the HS layer is twice the radius of gyration (RG). (J) Top view of HS proteoglycan distribution. Scale bars = 50 nm. (K) Schematic drawing of the different lengths of HS chains produced by genetically engineered MV3 and B16F10 cells. Data are presented as the mean ± SD, *P < 0.05, **$P < 0.005$, ***$P < 0.0005$.

but not their density. The average distance between the proteoglycans was approximately 220 nm for MV3 cells and 180 nm for B16F10 cells (Fig. 3E, F). Using our recently established nanoparticle-based titration method [8], we were able to calculate the average contour length of the HS chains (Fig. 3G, H). HS behave like a worm-like chain with a persistence length of 2.08 nm [35]. Accordingly, the diameter of the coiled HS chain at the surface of the melanoma cells was 20 ± 0.2 nm (B16F10 cells) and 26 ± 0.2 nm (MV3 cells). A scaled schematic drawing of our analysis is shown in Fig. 3I–K.

Loss of HS attenuated binding of vWF to the melanoma cell surface

Next, we analyzed the binding of vWF to the genetically engineered melanoma cells (Fig. 4A–D). We found a strongly reduced vWF binding after EXT1 knockdown or knockout. Moreover, the

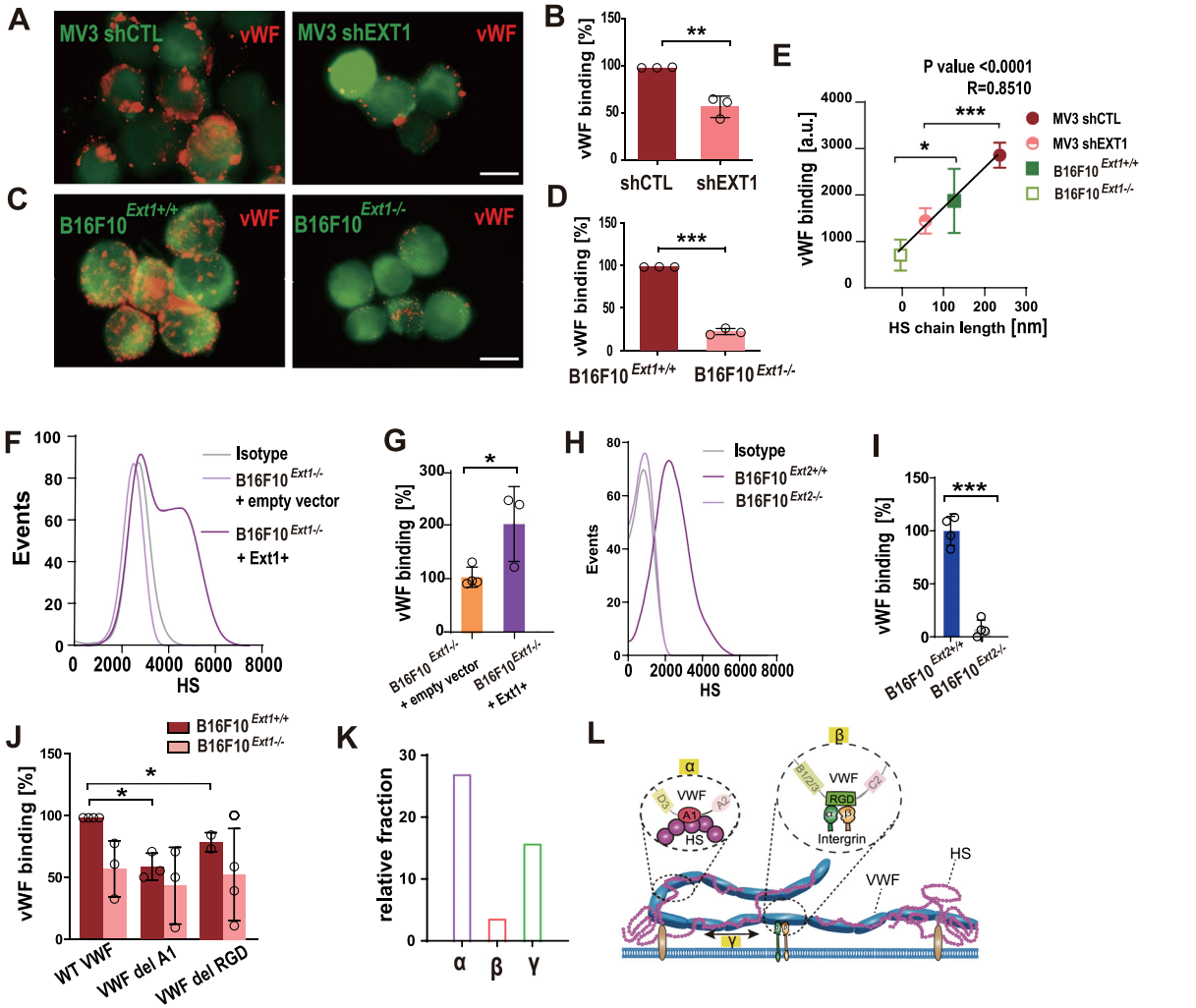

Fig. 4. Binding of vWF to melanoma cells was attenuated by loss of HS. (A) Less vWF bound to the surface of MV3 cells with a reduced HS synthesis (shEXT1). (B) Quantification of vWF binding by on-cell ELISA ($n = 3$). (C) Less vWF bound to the surface of B16F10$^{Ext1-/-}$ cells in comparison to B16F10$^{Ext1+/+}$ cells. (D) Quantification of vWF binding by on-cell ELISA ($n = 3$). Scale bars = 10 μm. (E) Linear relationship between HS chain length and vWF binding ability. (F) Flow cytometry showed the reoccurrence of HS in Ext1 rescued B16F10$^{Ext1-/-}$ cells after knock in of Ext1. (G) Restored vWF binding in Ext1 rescued B16F10$^{Ext1-/-}$ cells was quantified by on-cell ELISA. (H) Flow cytometry showed that the knockout of Ext2 abolished HS expression (B16F10$^{Ext2-/-}$ cells). (I) Quantification of vWF binding to B16F10$^{Ext2+/+}$ and B16F10$^{Ext2-/-}$ cells by on-cell ELISA ($n = 4$). (J) Binding of mutated recombinant vWF to B16F10$^{Ext1+/+}$ and B16F10$^{Ext1-/-}$ cells was quantified by on-cell ELISA ($n = 3$). (K) Basing on the data shown in (J), the applied binding model (Table S1) distinguished between purely HS dependent vWF binding (α), HS-independent vWF binding to integrins (β) and HS-dependent vWF binding to integrins (γ). Calculated contribution of α, β, γ are shown as bar diagram. (L) Schematic drawing of the interaction between HS, integrins, and vWF. Data are presented as the mean ± SD, $^{*}P < 0.05$, $^{**}P < 0.005$, $^{***}P < 0.0005$.

capacity to bind vWF was linearly dependent on the HS chain length (Fig. 4E). To exclude that potential off-targets of our CRIPSR/Cas9 approach contribute to the reduced vWF binding capability, we rescued the B16F10$^{Ext1-/-}$ by knock in of EXT1 (B16F10$^{Ext1-/-;Ext1+}$). The reoccurrence of HS at the cell surface (Fig. 4F) restored the ability to bind vWF (Fig. 4G). Also the disruption of HS biosynthesis by deleting Ext2 (Fig. 4H) abolished vWF binding (Fig. 4I). Interestingly, B16F10 cells with silenced HPSE expression (B16F10 shHPSE) showed an enhanced vWF binding capability (S-Fig. 3).

Although our data suggested a less pronounced role of integrins in binding soluble vWF, we aimed to study the triangular interaction between HS, integrin and vWF in more detail using mutated vWF in combination with the engineered melanoma cells (Fig. 4J). To better understand the obtained results,

we assumed that HS is able to promote integrin function in an additive manner and calculated the impact of HS and integrin on vWF binding (Table S1). As shown in Fig. 4K, our calculations indicate that the HS-related vWF binding (α) is more relevant than the integrin-related binding (β and γ).

We illustrated our findings in a schematic drawing (Fig. 4L). We assumed that long HS chains can interact with multiple A1 domains leading to a tight molecular complex between HS and the multimeric vWF comparable to a tape of hook and loop fastener. This complex formation has to be accompanied with a stretching of the HS chain and vWF. To obtain experimental evidence for this assumption, we aimed to determine whether cell surface bound vWF expose unoccupied A1 domains. Therefore, we probed the A1 domain of our vWF encapsulated melanoma cells with platelets. Platelets can potentially bind to A1 domains via their glycoprotein Ibα. However, as shown in S-Fig. 4A,B, overall rate of platelet binding was low and the presence of vWF at the cell surface had no impact on the binding rate suggesting that most of the A1 domains are occupied by HS.

HS-mediated enclosure of melanoma cells by vWF attenuated metastasis

To understand the biological relevance of vWF accumulation at the melanoma cell surface, we injected B16F10$^{Ext1+/+}$ cells and B16F10$^{Ext1-/-}$ cells into the tail vein of C57BL/6 wild type mice and analyzed the formation of lung metastasis (Fig. 5A). B16F10$^{Ext1-/-}$ cells formed significantly more metastases than the control cells (B16F10$^{Ext1+/+}$). To understand whether vWF binding to B16F10$^{Ext1+/+}$ cells was responsible for the reduced number of lung metastasis, we repeated the experiments in vWF deficient animals. In animals lacking vWF, B16F10$^{Ext1+/+}$ cells formed as much metastasis as B16F10$^{Ext1-/-}$ cells (Fig. 5B), indicating that the anti-metastatic effect of vWF was abolished. Corresponding quantifications are presented in Fig. 5C. To prove whether HS deficiency persist *in vivo*, we measured the levels of HS within metastatic foci (Fig. 5D,E). As expected, HS was barely detectable in metastases formed by B16F10$^{Ext1-/-}$ cells when compared to foci of control cells. Our results suggest that binding of plasmatic vWF to blood flowing melanoma cells attenuated metastasis, whereas lack of HS at the cellular surface of B16F10 cells facilitated metastasis.

Next to animal models, we also collected human tissue samples of primary melanomas and metastases. Immunofluorescence analysis indicated that melanoma cells within the primary tumors express higher HS levels than metastasized melanoma cells (Fig. 5F,G). We surveyed public transcriptome data sets [36,37] to analyze the expression of HS-related genes in primary melanomas and metastases (Figs. 5H and S-5A). EXT1 and SDC1 expression was significantly lower in metastatic foci when compared to the primary melanoma tissue. Decreased EXT1, SDC2, SDC3, and SDC4 expressions were also associated with a reduced patients' survival (Figs. 5I and S-5B). In summary, analysis of melanoma patients' biopsies and transcriptome data confirmed that melanoma cells expressing less HS were prone to metastasize.

To further prove the clinical relevance of our findings, we aimed to study the crosstalk between vWF and genuine patient-derived CTCs. Because no cultured melanoma-patient derived CTCs exists, we used CTC-ITB-01 cells previously isolated from a metastatic breast cancer patient [38]. In comparison to the common breast cancer cell line MDA-MB-231, CTC-ITB-01 expressed only very low HS levels (Fig. 5J), which corresponds also to a low vWF binding capacity (Fig. 5K). This result further suggests that lower HS expression and a reduced ability to bind vWF is associated with metastatic CTCs.

HS bound vWF attenuates adhesion of cancer cells to the vascular endothelium

Our data indicate that plasmatic vWF recognize blood flowing melanoma cells through binding to HS. In the next set of experiments, we aimed to elucidate, whether vWF sealing of cancer cells affected their adhesion to the vascular endothelium. Therefore, we used microfluidic experiments mimicking pathophysiological vascular conditions [14,39]. In the present setup, we stimulated the endothelial cells with recombinant TNFα promoting a tumor-like proinflammatory and proadhesive microvascular environment. Endothelial cells were perfused simultaneously with green fluorescent B16F10$^{Ext1+/+}$ cells and red fluorescent B16F10$^{Ext1-/-}$ cells in the absence or presence of plasmatic vWF (Fig. 6A). In line with our animal experiments, presence of vWF prevented the vascular adhesion of B16F10$^{Ext1+/+}$ cells but not of B16F10$^{Ext1-/-}$ cells (Fig. 6B). We found similar relationships in microfluidic experiments with the human melanoma cell line MV3 and patient-derived CTC-ITB-01 (S-Fig. 6A−D).

Additionally, we measured that in the absence of vWF, B16F10$^{Ext1-/-}$ cells bound more frequent to the endothelial cell layer than the B16F10$^{Ext1+/+}$ cells (Fig. 6B). We performed electric cell-impedance sensing (ECIS) (Fig. 6C, D) and reflection interference contrast microscopy (RICM) (Fig. 6E, F) to understand this effect. The results of ECIS and RICM indicate that HS deficient B16F10 cells approach significantly closer to their substratum than the control cells. The corresponding thickness of the cellular HS layer was in the 20 nm range (Fig. 6G), which is in good agreement with our results obtained by nanoparticle titration (Fig. 3I). These findings point towards a repulsive effect of the melanoma cell glycocalyx, which counteracts

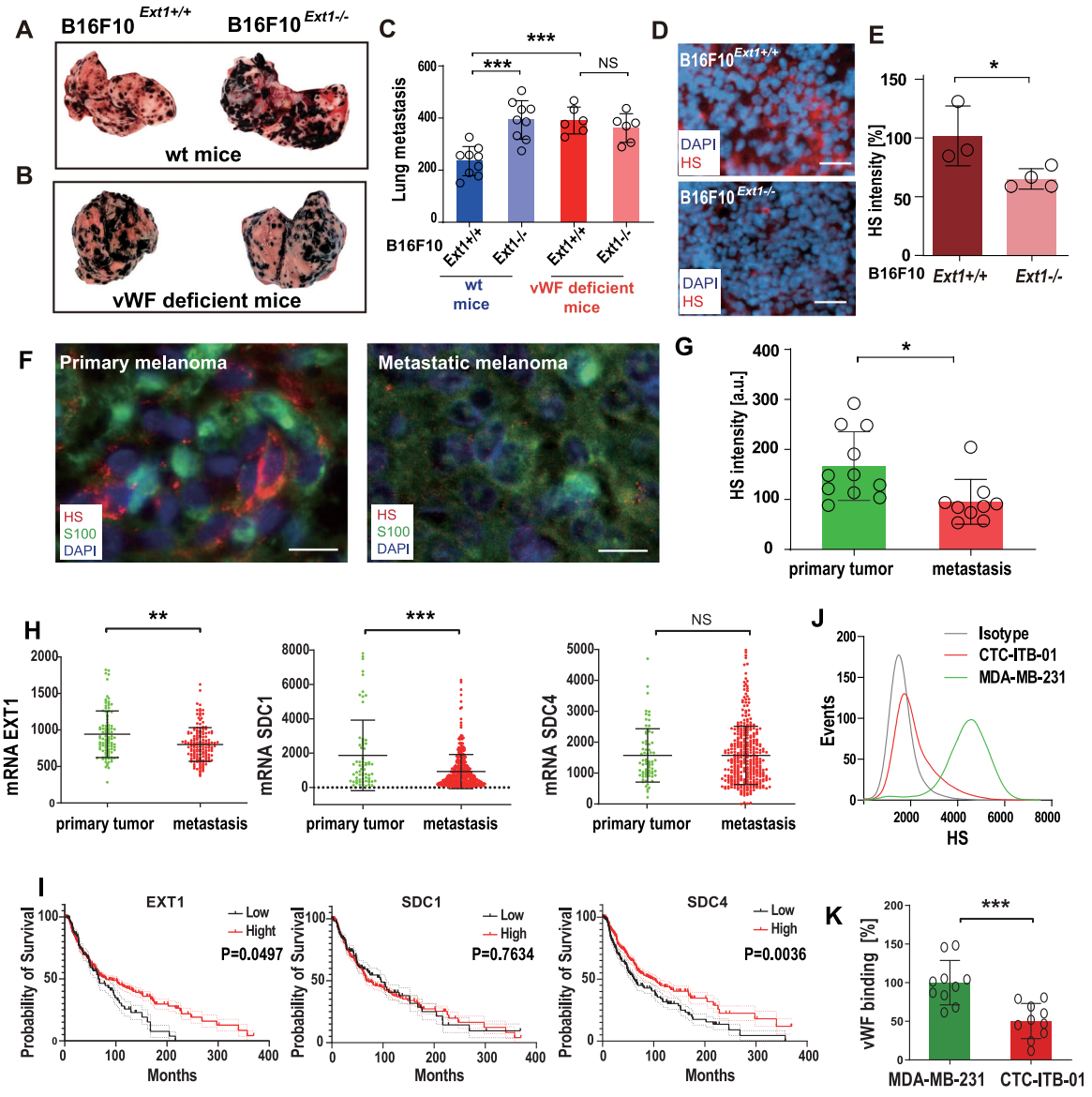

Fig. 5. Binding of vWF to melanoma cells reduced lung metastasis. (A) Representative images of metastatic lungs of wild type (wt) mice. (B) Representative images of metastatic lungs of vWF deficient mice. (C) Quantification of metastatic foci numbers (n = 5). (D) HS expression in the metastatic foci of wt mice. Scale bars = 100 μm. (E) Quantification of HS staining intensities in the analyzed tissues (n = 4). (F) Immune fluorescence staining of human primary melanoma and metastatic tissue. Scale bars = 20 μm. (G) Quantification of HS fluorescence intensity in primary tumors (n = 11) and metastases (n = 9). (H) Expression levels of EXT1, SDC1 and SDC4 measured in melanoma tissues of metastatic foci or primary tumors (n = 441). Data were obtained from the public transcriptome database cBioportal. (I) Correlation between melanoma patients' survival and the expression of EXT1, SDC1 and SDC4 are presented as Kaplan-Meier diagram (n = 441). (J) HS expression in the breast cancer cell line MDA-MB-231 and circulating breast cancer cell line CTC-ITB-01 was measured by flow cytometry. (K) Binding of vWF to breast cancer cells was quantified by fluorescence microscopy (n = 10). Data are presented as the mean ± SD, $^{*}P < 0.05$, $^{**}P < 0.005$, $^{***}P < 0.0005$.

vascular adhesion and which might be further enhanced through the accumulation of plasmatic vWF.

vWF promotes vascular repulsion

Previous literature suggested Thy1, P-selectin and vascular cell adhesion protein 1 (VCAM1) as relevant endothelial adhesion molecules [40–42]. Thy1 can interact with $\alpha_v\beta_3$ integrins, P-selectin can interact with sialy-lewis-X. VCAM1 is the receptor for very late antigen 4 (VLA4) which is also expressed by B16F10 cells (S-Fig. 7A). VCAM1 was expressed in our endothelial cells whereas Thy1 and P-selectin expressions were below the detection limit (S-Fig. 7B). In line with that, interference of the potential

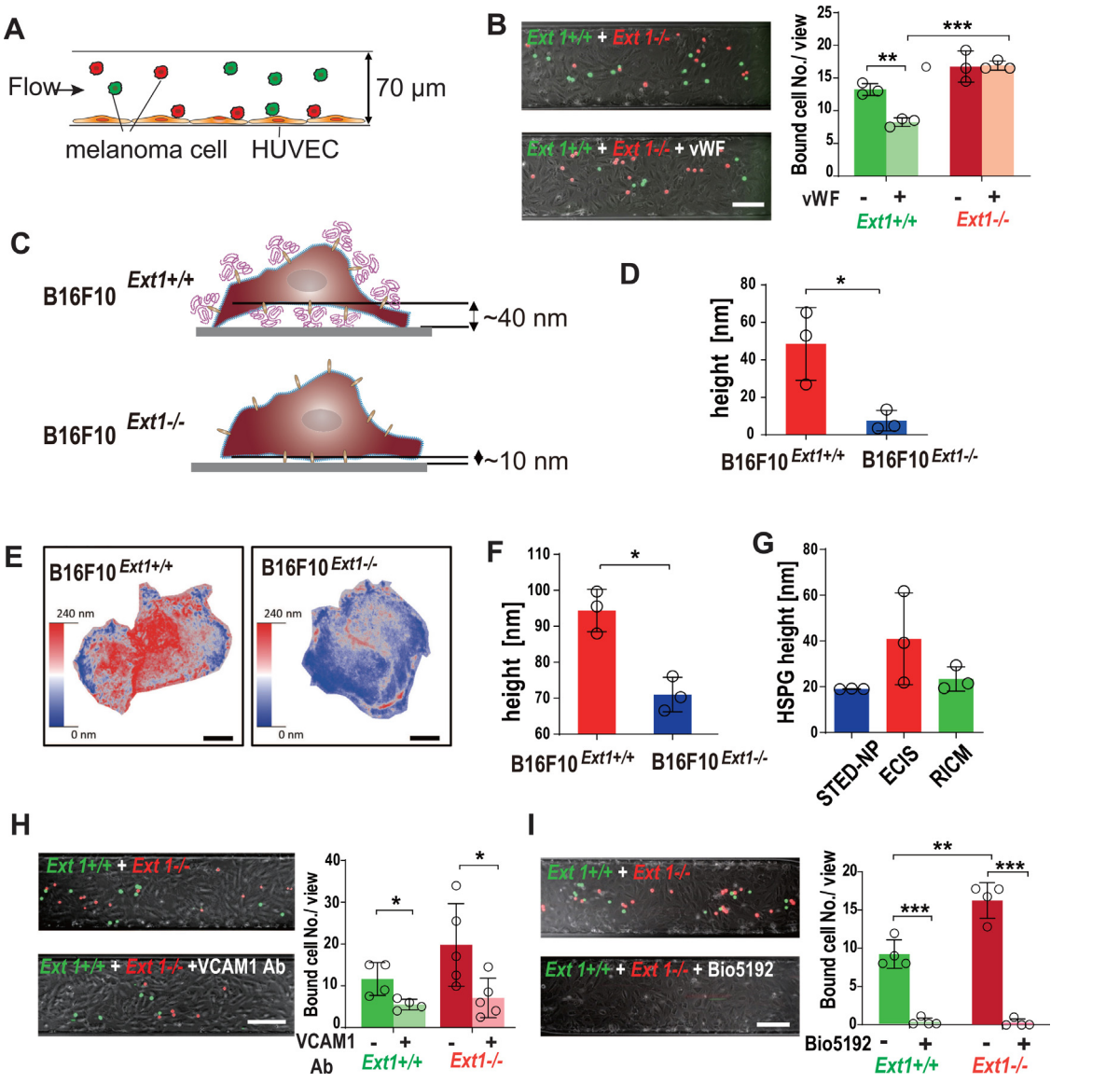

Fig. 6. VWF attenuated B16F10 cell adhesion to endothelial cells. (A) Schematic drawing of the microfluidic setup. (B) Attached B16F10$^{Ext1+/+}$ (green) and B16F10$^{Ext1-/-}$ (red) cells on HUVECs in the absence or presence of vWF. Quantification of cell adhesion is shown as bar diagram (n = 3). (C) Schematic drawing of the B16F10 cell adhesion to fibronectin-coated surfaces. The HS layer in the B16F10$^{Ext1+/+}$ cells hinders a tight contact to the surface (D) Calculated distance of the ventral side of the B16F10$^{Ext1+/+}$ cells and the B16F10$^{Ext1-/-}$ cells to the substratum by ECIS measurements. (E,F) Distance of the adhering B16F10 cells to the substratum was measured by RICM. Scale bars = 5 µm. (G) Comparison of the HS layer thickness measured by STED/nanoparticle titration, ECIS, and RICM. Data are presented as the mean ± SD, $^*P < 0.05$. (H) B16F10 cell adhesion was blocked by vascular cell adhesion protein 1 (VCAM1) neutralizing antibodies. Quantification of cell adhesion is shown as bar diagram (n = 5). (I) B16F10 cell adhesion was blocked by the VLA4 inhibitor Bio5192. Quantification of cell adhesion is shown as bar diagram (n = 4). (B,H and I) Scale bars = 200 µm. Data are shown as the mean ± SD, $^*P < 0.05$, $^{**}P < 0.005$, $^{***}P < 0.0005$.

Thy1-$\alpha_v\beta_3$ integrin interaction by cilengitide was ineffective to attenuate melanoma cell adhesion (S-Fig. 7C,D). Data shown in S-Fig. 7E, and F indicate that also the contribution of P-selectin was negligible. In contrast, blocking of VCAM1 by neutralizing antibodies (Fig. 6H) or inhibition of VLA4 by Bio5192 (Fig. 6I) prevented melanoma cell adhesion indicating that the binding of B16F10 cells to the endothelium was mostly VCAM1/VLA4 dependent.

To mimic the approach of melanoma cells to the endothelium and to measure the acting molecular forces, we applied single molecular force spectroscopy (SMFS) as illustrated in Fig. 7A. Recombinant VCAM1 and VLA4 was covalently linked to glass

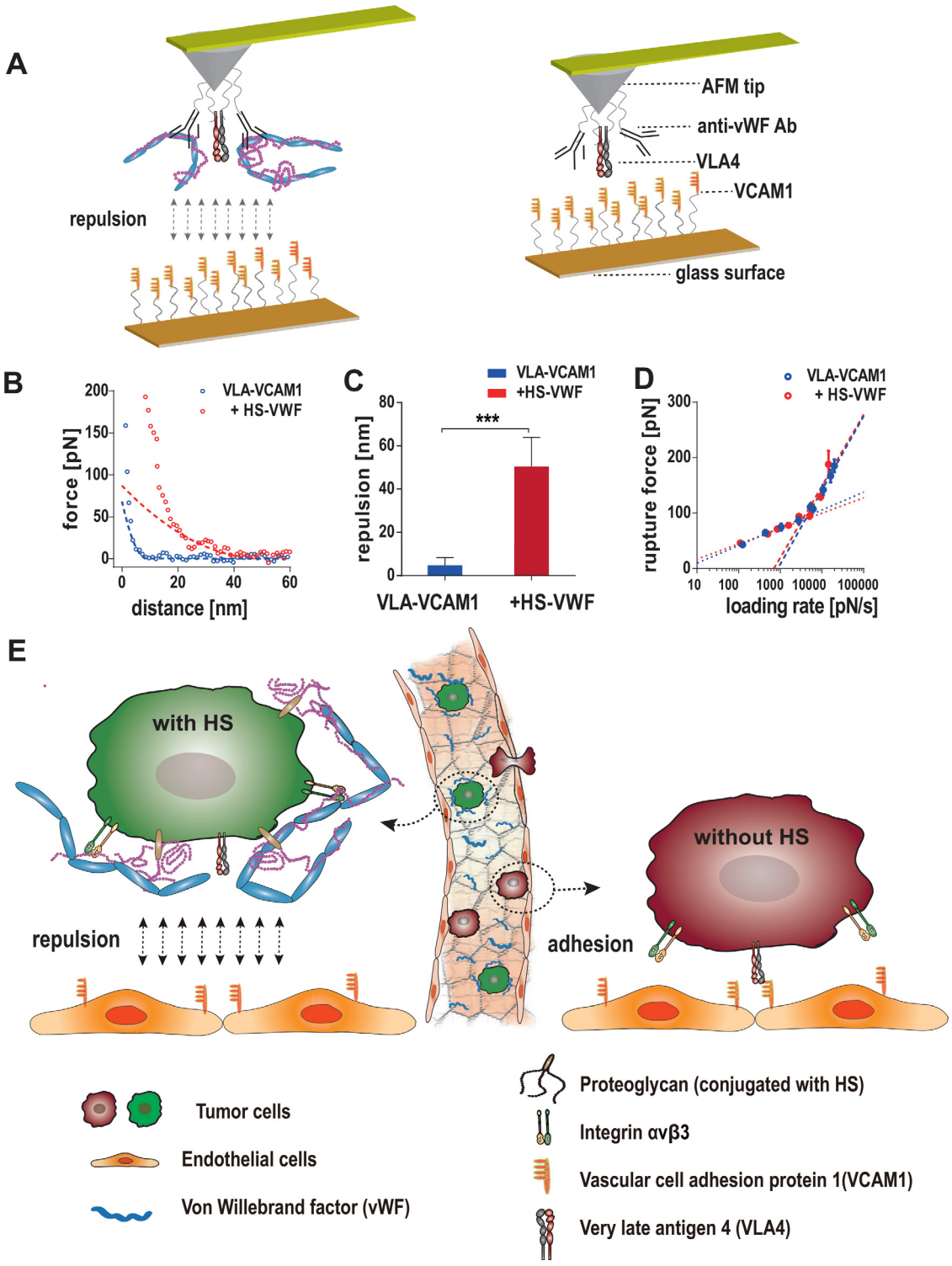

Fig. 7. VWF promotes vascular repulsion. (A) Schematic drawing of single-molecule force spectroscopic (SMFS) experiments. Recombinant VCAM1 and VLA4 were covalently linked to glass slides or atomic force microscopy tips. Where indicated, a preformed complex of vWF and HS was attached to the tip via a covalently linked antibody. We approached the functionalized tip to the surface and recorded the force required to contact the surface. (B) Force-distance curves recorded during the approach of the SMFS probe to the surface. Dashed lines show the curve fitting according to the Hertz model to determine the onset of repulsion. (C) Quantification of the onset of repulsion. (D) Rupture force required to dissociate the bond between VCAM1 and VLA4. The first energy barrier was characterized by a bond life time

slides or atomic force microscopy (AFM) tips, respectively. Where indicated, we attached additionally a complex of vWF and HS to the VLA4 functionalized AFM tip via a covalently linked vWF antibody. As shown in Fig. 7B, we measured strong repulsive forces between the glass slide and the functionalized AFM tip after adding the vWF-HS complex. The onset of repulsion shifted from 5 ± 3.6 nm (without vWF-HS) to 51 ± 13.4 nm (with vWF-HS) which is in the size range of vWF [43] (Fig. 7C).

To further investigate the molecular connection between VCAM1, VLA4, vWF and HS, we measured the rupture force required to dissociate VCAM1 and VLA4 at different loading rates (Fig. 7D, blue circles). In line with Zhang et al. [44], we identified two energy barriers that govern the interaction between VCAM1 and VLA4 (Fig. 7D). As indicated by the linear regression lines, we found that the close proximity of the vWF-HS complex had only a very limited impact on the VCAM1-VLA4 interaction. That vWF cannot competitively prevent the interaction of VCAM1 to VLA4, was also confirmed by measurements with surface acoustic wave (SAW)-driven biosensors (S-Fig. 8). Specificity of our AFM measurements was confirmed in control experiments with a VCAM1 neutralizing antibody (S-Fig. 9).

Taken together, our biosensor and SMFS measurements suggest that vWF cannot directly interfere with the VLA-VCAM1 interaction. However, accumulation of vWF at the cancer cell surface enhances the repulsive power of the HS layer, which in turn prevents vascular adhesion and metastasis (Fig. 7E).

Discussion

In the present work, we investigated the impact of plasmatic vWF on melanoma metastasis. Melanoma cells with a pronounced HS expression and thus with a large vWF binding capacity showed a reduced potential to form vascular metastasis. This indicates anti-metastatic properties of plasmatic vWF. Melanoma cells with a reduced HS expression evade recognition by vWF and were privileged to form metastasis as their adhesion to the vascular endothelium was increased. *Vice versa*, it was shown that melanoma cells with increased HS levels, due to a suppressed expression of HPSE, metastasized less to the lung [45,46].

In the present work, we found that B16F10 cells adhere to the endothelium through the VLA4/VCAM1 axis, whereas the previously reported interaction between Thy1 and $\alpha_v\beta_3$ integrin appeared to be less relevant [40]. Interestingly, vWF interfered not directly with the VLA4/VCAM1 interaction but enhanced the repulsive power of the melanoma cell glycocalyx. We found that the glycocalyx of melanoma cells is largely composed of HS chains with a length of 100−200 nm producing a glycocalyx layer with a thickness of approximately 20 nm. Experiments with mutated vWF indicated that the interaction between vWF and HS at the melanoma cell surface required the presence of the A1 domain. In its globular conformation, vWF hides the A1 domain, whereas stretching of vWF e.g. through shear forces promote the exposure of the A1 domain. This suggests that during the interaction with the melanoma cell surface, vWF is at least partially elongated. Previous molecular dynamic simulations demonstrated that the high molecular weight of vWF facilitate the transient and only partial elongation of vWF [47]. Overwhelming secretion of vWF by tumoral endothelial cells in combination with a lack of active ADAMTS13 (a disintegrin−like and metalloproteinase with thrombospondin type 1 motif 13) was shown to promote extensive vWF stretching and formation of Ultra-large vWF (ULvWF) fibers. Although mechanistic data are missing, ULvWF fibers were postulated to promote metastasis by anchoring CTCs at their site of metastasis [24,48]. This suggests a dual function of vWF. In a balanced physiological situation in which ULvWF fibers are barely formed, plasmatic vWF may prevent metastasis. In a more unbalanced homeostatic situation, present e.g. in tumors or tumor-primed tissues, ULvWF fiber formation might be favored [49]. Whether ULvWF fibers can directly contribute to metastases is unclear and further research is required to identify molecular interaction partners.

In the present study, we confirmed that plasmatic vWF is able to bind to CTCs through HS. We showed that the length of the HS chain is relevant for the binding of vWF. Further studies are required to investigate the potential impact of the HS chain sulfation as a known regulator of HS-protein interactions [50]. Interestingly, integrins contribute less to the binding of soluble vWF than HS. Moreover, our data indicate that the binding activity of integrins was even largely dependent on HS. The molecular interplay between the glycocalyx of cancer cells and integrins has previously been proposed. The HS exposing proteoglycan SDC4 or SCD1 were shown

(τ1) of 0.066 ± 0.006 s and a bond length (x1) of 0.70 ± 0.03 Å. The second barrier was characterized by a bond life time (τ2) of 2.8 ± 0.32 s and a bond length (x2) of 3.0 ± 0.06 Å. After coupling the vWF-HS complex to the VLA4-functionalized tip, bond life times and bond lengths were only slightly affected (τ1 = 0.053 ± 0.006 s; x1 = 0.51 ± 0.03 Å; τ2 = 3.3 ± 0.79 s and x2 = 3.0 ± 0.10 Å). (E) Schematic presentation of the interference of vWF with the binding of melanoma cells to the vascular wall. Data are shown as the mean ± SD, *$P < 0.05$, **$P < 0.005$, ***$P < 0.0005$.

to directly promote $\alpha_v\beta_3$ or β_5 integrin activation [51,52]. Others postulated that especially long glycan chains can activate integrins through an energetic trap formation [12]. Most of the previous research investigated the cross talk between the glycocalyx and integrins in the context of cell adhesion under static conditions. We studied the triangular communication between integrins, HS and vWF in suspension and dynamic flow conditions.

We concluded from our data that HS together with integrins orchestrate the binding of soluble vWF. In the present study we focused mainly on the human melanoma cell line MV3 and the murine melanoma cell line B16F10. Although it is likely that other cancer cells are also able to bind vWF through HS, extend and biological relevance of vWF accumulation might be different. Moreover, to which extend other plasma proteins are recognized by HS in concert with integrins remained to be clarified. Indeed, HS is a known interaction partner of various plasma proteins comprising cytokines, complement factors or members of the coagulation system [53]. However and in contrast to all other plasma proteins, vWF is a very large multimer in the gigadalton range. Even after partial degradation by ADAMTS13, blood circulating vWF multimers are composed of about 200 monomers [54]. Because every monomer has a binding site for HS, vWF multimers have an enormous potential to form a tight complex particularly with long HS chains. In line with the supposed complex between HS chains and multimeric vWF, cell surface bound vWF was inaccessible for platelets. This suggests a lack of free A1 domains but also an irreversible character of the HS-vWF complex. Our experiments with MV3-spiked blood showed that vWF accumulated mainly around melanoma cells but not leucocytes. The origin of this selective binding might be related to the different HS composition at the leucocyte surface [55–57].

In summary, we showed that HS-mediated recognition of cancer cells by plasmatic vWF can reduce metastasis. This suggested that the administration of vWF to tumor patients during events that may lead to an increased release of CTCs into the circulation (e.g., tissue biopsies, surgery or radiation [58,59] may counteract hematogenous metastasis. Because the exclusive application of vWF may favor the formation of ULvWF leading to thrombotic events and thus a reduced patients' benefit, a co-administration of ADAMTS13 appeared to be more advisable. Also the tailored manipulation of the glycocalyx of CTCs through cell surface adhesive HS mimetics or inhibition of CTC-expressed HPSE activity might show anti-metastatic potentials. Although our present investigation was focused on melanoma metastasis, our additional data on breast cancer CTCs suggest that we have discovered a more general anti-metastatic mechanism.

Experimental procedures

Mouse procedures and patients' tissues

All animal experiments were approved by the governmental animal care authorities ("Behörde für Justiz und Verbraucherschutz, Hamburg" project N033/2022). C57BL/6J mice and vWF deficient mice (Jackson Laboratory) were maintained under specific pathogen free conditions. B16F10 melanoma cells were i.v. injected into 8-12 week old mice (1×10^6 cells per mouse). After 15 days, metastatic foci were counted and lungs were embedded for cryosectioning (Tissue-Tek O.C.T. Compound).

The usage of patient samples was approved by the ethics committee of the University Medical Center Hamburg-Eppendorf (approval no.: MC-028/08). Melanoma tumor tissues were obtained from stage UICC III and IV malignant melanoma patients.

Melanoma patients' data

RNAseqV2 gene expression and clinical data of skin cutaneous melanoma patients were publicly accessible through the cancer genome atlas (TCGA) project [60]. Altogether, data of 441 cutaneous melanoma patients were analyzed comprising 169 females and 273 males. The average age of the included patients was 58 $\pm$ 16 years. 81 samples were originated from primary melanomas, while 367 samples are collected from metastases. Further information is publicity available on the cBioportal repository [37,61] and the related original research [60]. Kaplan-Meier plots were generated to illustrate the relationship between patients' overall survival and gene expression levels.

Microfluidic experiments

Human umbilical vein endothelial cells (HUVECs) were seeded and grown to confluence in Leibovitz's L-15 Medium (gibco 31415029) on fibronectin coated BIOFlUX 200 48-WELL plates (Fluxion) at 37 °C. Prior to the experiment, HUVECs were stimulated with 10 ng/mL TNFα (R&D systems) for 4 h. Tumor cells with or without vWF (20 μg/mL), VCAM1 (100 μg/mL, Abcam), Bio5192 (100 μM, TOCRIS), Cilengitide (10 μM, Merck) were perfused at a shear force of 2 dyn/cm^2 using the BIOFLUX200 system (Fluxion). Adherent cancer cells were counted by fluorescence microscopy (Observer z.1, Zeiss).

Dynamic adhesion to murine P-selectin under physiological flow conditions was analyzed in a laminar flow adhesion assay as previously described [41,62]. Briefly, ibidiTreat μ-slide IV$^{0.4}$ flow chambers (ibidi GmbH) were incubated with 20 μg/mL

recombinant murine P-selectin/IgG1-Fc chimeras (rmP-Sel, from R&D Systems) 30 min prior to the flow adhesion assay (tumor cell suspension: 1×10^5 cells/mL; flow rate: 8.5 mL/h; shear stress: 0.25 dyn/cm^2). IgG1-Fc fragments served as negative control (R&D Systems). Data were acquired and evaluated with CapImage software (version 8.6, Dr. Heinrich Zeintl, Heidelberg).

Binding of vWF to cells by on-cell ELISA and immunofluorescence analysis

500,000 cells in PBS containing calcium and magnesium were incubated with or without wt vWF (40 μg/mL), mutated vWF (40 μg/mL), Cilengitide (10 μM) and Tinzaparin (100 U/mL) at 37 °C for 30 min. Cells were fixed in 4% PFA for 10 min, washed and blocked with 1% BSA. For on-cell ELISA, Cells were stained by horse reddish peroxidase-Rabbit anti human (Dakocytomation, 1:2000) for 30 min at RT. After washing, cells were resuspended with 100 μl PBS and transferred into 96-well plates. 100 μl TMB substrate (R&D System) was used for detection. Enzyme reaction was stopped by adding 50 μl 1M H_2SO_4. Optical densities were determined in each well at 450 and 540 nm using a microplate reader (BioteK PowerWave XS2 photometer).For immunofluorescence analysis, cells were incubated with the first antibody (rabbit anti-human VWF, Dakocytomation, 1:250) for 30 min at RT. After washing, cells were incubated with the second antibody (Alexa 647-conjugated goat anti-rabbit, Thermo Fisher Scientific, 1:2000) for 30 min at RT. Cells were washed and resuspended in 30 μl Fluoromount G (Southern Biotech). A drop of the cell suspension was deposited on a glass slide and covered with a coverslip. Fluorescence microscopy was performed using a Zeiss Observer z.1 microscope. Images were analyzed with Image J.

Whole human blood spiked with MV3

5-Chlormethylfluoresceindiacetat-labeled (Thermo Fisher Scientific, 1:1000) MV3 cells were washed and incubated with whole blood at 37 °C for 30 min. The buffy coat containing melanoma cells and leucocytes was isolated by density gradient centrifugation using ficoll as previously reported [63]. vWF was detected by rabbit anti-human VWF (Dakocytomation, 1:250) and Alexa 647-conjugated goat anti-rabbit (Thermo Fisher Scientific, 1:2000) antibodies. Nuclei were stained with DAPI. Fluorescence microscopy was performed using a Zeiss Observer z.1 microscope. Images were analyzed with Image J.

Surface acoustic wave biosensor

Surface acoustic wave (SAW) measurements were performed to detect binding of vWF to His-tagged VLA4 (R&D systems, Minneapolis, USA). For that, a Sam5 Blue SAW biosensor (SAW Instruments GmbH, Munich, Germany) was applied. A VLA4 containing model membrane of 20 mol% DGS-NTA (Ni) and 80 mol% DPPC (Sigma Aldrich) at the sensor surface was prepared as described before [64]. A buffer flow (40 μL/min) for baseline equilibration was used. Afterwards, 2 μg rh His-tagged rh His-tagged VLA4 was injected with a flow rate of 20 μL/min for binding of the His-tag to the DGS-NTA (Ni) lipid in the membrane. Subsequently, a dilution series of vWF between 0.85 and 137 nM in running buffer (1 mM $CaCl_2$, 1 mM $MgCl_2$, 0.5 mM $MnCl_2$) was injected for measurements.

STED microscopy, nanoparticle titration and glycocalyx degradation

STED microscopy experiments were conducted under similar conditions as previous studies [8]. Briefly, imaging was carried out in sequential line scanning mode using an Abberior STED expert line microscope. A pulsed laser was used for excitation at 640 nm and a near-infrared pulsed laser (775 nm) for depletion. Images were recorded with a dwell time of 3 μs and the voxel size was set to $20 \times 20 \times 150$ nm. Images were acquired in time-gating mode with a gating width of 8 ns and a delay of 781 ps. Nanoparticle titration was conducted to measure the length of the HS chains as previous reported [8]. In Brief, after digestion with 150 mg/mL hyaluronidase (Sigma-Aldrich) and 500 mU/mL chondroitinase ABC (AMS Biotechnology) for 3 h at 37 °C, 400,000 cells were incubated with fluorescent chitosan nanoparticles at different concentrations (1.12×10^{11}, 2.24×10^{11}, 4.48×10^{11}, 8.96×10^{11}, 1.78×10^{12} particles per mL) for 30 min at 37 °C. In control experiment, cells were treated with 500 mU/mL heparinase I and II (Sigma-Aldrich). After washing, the cells were resuspended in 500 μL PBS. Nanoparticle binding was measured by flow cytometry. Dose-response curves and STED images were used to calculate the length of the HS chain.

Gel chromatography

Subconfluent cell cultures were incubated with 200 μCi/mL ^{35}S-sulfate (Perkin Elmer). After 24 h, the medium was removed, the cell layers washed twice with PBS and treated with 1 mg/mL trypsin for 5 min at 37 °C. Free glycosaminoglycan chains were isolated from the trypsin fraction (derived from cell surface/matrix proteoglycans) as described [33]. CS was degraded with chondroitinase ABC (Seikagaku) in 50 mM Tris-HCl pH 8.0, 30 mM Na-acetate

and 0.1 mg/mL bovine serum albumin. HS was degraded by nitrous acid treatment at pH 1.5 with 0.5 M HNO2 which cleave *N*-sulfated glucosamine units [65]. Chain length was analyzed by gel chromatography on a Superose 6 HR10/30 column (Amersham Biosciences) eluted with 0.5 M NH_4HCO_3. Fractions were collected at 1 min intervals and the radioactivity was monitored by liquid scintillation counting. The elution positions of molecular-weight standards derived from heparin (8.3 kDa) and hyaluronan (19, 30, 43 and 210 kDA) are indicated in Fig. 3I,L.

Electric cell-impedance sensing (ECIS)

ECIS was performed as previously reported [8]. Briefly, gold electrodes (8W10E+ PET, Applied Biophysics, New York, USA) were coated with fibronectin (10 μg/mL) for two hours and 200,000 B16F10 cells were seeded per well. Impedance spectra ranging from 500 to 64,000 Hz were recorded every 48 s for 24 h (ECIS Z theta, Applied Biophysics, New York, USA). Measurements were performed in an incubator with humidified atmosphere and 5% CO_2 at 37 °C. Distance of the cells from its substrate were calculated assuming an rectangular cell shape as previously shown by Giaever and Keese [66].

Reflection interference contrast microscopy (RICM)

B16F10 cells (50,000/well) were seeded into an eight-chamber microscopy slide (ibidi GmbH) coated with fibronectin (100 μg/ml). Immediately after seeding, the slide was placed on the RICM stage (z1 Observer, Zeiss, Oberkochen, Germany) for continuous imaging. During microscopy, cells were maintained at 37 °C in a humidified atmosphere containing 5% CO_2. Distance of the ventral side of the cell to the microscopy slide was determined at a wavelength (λ) of 480 nm. Mean light intensity per cell (I_{cell}), minimum light intensity per cell (I_{min}), maximum light intensity per field of view ($I_{max,fov}$) and minimum light intensity per field of view ($I_{min,fov}$) was determined by Image J. The average distance (d) of the adhering melanoma cells from the substratum was calculated by $d = (I_{cell} - I_{min})\ \lambda / 2(I_{max,fov} - I_{min,fov})$.

Single molecule force spectroscopy (SMFS)

SMFS measurements were performed with an atomic force microscope (AFM) (NanoWizard, JPK) as previously reported [67]. AFM tips (CS38/No Al, μMasch) and glass slides (Thermo Fisher Scientific) were functionalized with ethoxy silane polyethylene glycol (PEG) acid (Nanocs). Recombinant VLA4, VCAM1 (R&D systems, Minneapolis, USA) or anti-vWF antibodies (DAKO GmbH, Jena, Germany) at a concentration of 1 mg/mL were coupled to the PEG linker. Where indicated, complexes of recombinant human vWF and 1000 U/mL unfractionated heparin (Merck) were formed and attached to the AFM tip via the anti-vWF antibody. Rupture forces were recorded at different nominal loading rates ranging from 5000 to 160,000 pN/s. At least 500 force curves per loading rate have been analyzed. The bond lifetime (τ) and the bond length (x) for both energy barriers were determined [68]. The onset of repulsion was determined as previously reported [69].

Flow cytometry

Cells were collected and incubated with Alexa Fluor 647(or 488)-conjugated WGA (Thermo Fisher Scientific 1:1000) or HS directed antibodies (10E4 epitope, AMS Biotechnology, 1:1000) for 30 min on ice. After washing with PBS, HS antibodies were further labeled with Alexa Fluor 647 goat anti-mouse IgM secondary antibodies (Thermo Fischer Scientific, 1:1000) for 30 min on ice. Fluorescence signals were evaluated by flow cytometry (BD FACSCanto II, Biosciences). Data were analyzed by Flowing Software (version 2.5.1).

Static P-selectin binding of B16F10 cells was analyzed by flow cytometry as described before [41]. Briefly, 10 μg/mL recombinant chimeric murine P-selectin-IgG-Fc constructs (R&D Systems), precomplexed with biotin-linked anti-human IgG (Sigma-Aldrich) and allophycocyanin- (APC-) conjugated streptavidin (BD Bioscience) were used. Cells were incubated for 20 min at 4 °C with complexed selectins. IgG-Fc fragments (R&D Systems) served as isotype control. Data were generated with CyFlow Cube 8 (Sysmex) analyzer and evaluated with FCS Express 4 Flow software (De Novo Software).

Immunofluorescence staining

Cells and tissue cryosections (10 μm) were fixed in 4% PFA for 10 min, washed with PBS and blocked with 10% goat serum. The following primary antibodies were used: HS directed antibody (10E4 epitope, AMS Biotechnology, 1:1000), rabbit anti-human VWF (Dakocytomation, 1:250), Alexa 647 or 488-conjugated WGA (Thermo Fisher Scientific, 1:1000), integrin beta3 (Novus Biologicals 1:200), anti-S100 Protein rabbit polyclonal, serum (1:100). The following secondary antibodies were used: Alexa 647-conjugated goat anti-mouse (IgM; Thermo Fisher Scientific, 1:5000), Alexa 647-conjugated goat anti-rabbit (Thermo Fisher Scientific, 1:2000). Nuclei were stained with DAPI. Samples were imaged by fluorescence microscopy (Observer z.1, Zeiss). Images were analyzed with Image J (version 1.52) [70].

Genetic engineering of melanoma cells

EXT1 Human shRNA Plasmid Kit were purchased from origene, 4 unique human EXT1 shRNA and a scrambled shRNA were cloned into the pGFP-C-shLenti Vector lentiviral GFP vector. Virus particles and MV3 cell transduction was performed as previously reported [14]. Transduced cells were cultured with 2 μg/mL puromycin to select for stably transduced cells. sgRNAs were designed using the online CRISPR Design tool (http://crispor.tefor.net/).Target sequences of *Ext1* are 5′-CACCGAACATTC-TAGCGGCCATCGA-3′ and 5′-AAACTC-GATGGCCGCTAGAATGTTC-3′. sgRNAs were cloned into the pSpCas9(BB)-2A-Puro vector (Addgene #48139). Final vector constructs were transfected into the melanoma cells by Lipofectamine 2000 (Thermo Fisher Scientific) as previously reported [71]. Stable *Ext1* KO cell lines were generated by selection with puromycin (2 μg/mL). Single cell clones were picked through serial dilution of the puromycin-resistant cells in 96-well plates. Gene editing was confirmed by the Alt-R Genome Editing Detection Kit (Integrated DNA Technologies). Genetic alterations were further analyzed by Sanger sequencing using primers bracketing the targeted gene region (5′-GGAACCGTAGTGCTCTGCAC-3′ and 5′-GAACATGTGTCTCTCTGAGTCG-3′). Cell surface HS expression was detected by flow cytometry and immunofluorescence staining.

To rescue Ext1 knockout cells, full-length cDNA of the *Ext1* gene was cloned into the pLenti CMV/TO Puro vector (addgene #17482). Lentivirus particles and B16F10 cells were produced as previously reported [14]. HS expression in rescued melanoma cells was detected by flow cytometry. B16F10 cells with a silenced HPSE expression were produced and characterized as previously stated [45].

RNA extraction and qPCR

RNA was extracted using RNeasy Plus Mini Kit (Qiagen), and cDNA was synthesized by using Reverse Transcription System (Promega). qPCR reactions were performed using a real-time PCR system (Light cycler 96 system, Roche) and the GoTaq® qPCR Master Mix (Promega). The primers used for qPCR are provided in Supplementary Table 2.

Statistics

Statistical analysis was performed with GraphPad Prism 6 software and significance was tested by Student's t-test. All results are presented as means ± SD as indicated in the legend. $P < 0.05$ was considered as significant difference.

Data and materials availability

All data needed to evaluate the conclusions in the paper are present in the paper and/or the Supplementary materials.

Funding

This study was supported by the Heike und Wolfgang Mühlbauer Stiftung, Erich und Gertrud Roggenbuck-Stiftung, the European Union's Seventh Framework Program for Research, Technological Development and Demonstration under grant agreement 613931 and the Deutsche Forschungsgemeinschaft within the RTG 2099, the IRTG 1549, SFB/Transregio 23 and SHENC-Unit FOR 1543. The PhD position of Yuanyuan Wang was supported by the program of China Scholarship Council NO. 201608130093 and Hamburg Pro exzellenzia plus Stipendien-Program.

CRediT authorship contribution statement

Yuanyuan Wang: Writing – original draft, Methodology, Formal analysis, Investigation, Validation, Visualization. **Xiaobo Liu:** Methodology, Formal analysis, Writing – review & editing. **Tobias Obser:** Methodology, Resources, Writing – review & editing. **Alexander T. Bauer:** Methodology, Resources, Writing – review & editing. **Martin Heyes:** Methodology, Writing – review & editing. **Sarah Starzonek:** Methodology, Writing – review & editing. **Mina Zulal:** Methodology, Writing – review & editing. **Karena Opitz:** Methodology, Writing – review & editing. **Leonie Ott:** Methodology, Resources, Writing – review & editing. **Sabine Riethdorf:** Methodology, Resources, Writing – review & editing. **Tobias Lange:** Methodology, Writing – review & editing. **Klaus Pantel:** Methodology, Resources, Writing – review & editing. **Gerd Bendas:** Methodology, Writing – review & editing. **Stefan W. Schneider:** Methodology, Resources, Writing – review & editing. **Marion Kusche-Gullberg:** Methodology, Writing – review & editing. **Christian Gorzelanny:** Conceptualization, Writing – original draft, Formal analysis, Validation, Supervision.

Declaration of Competing Interest

The authors declare that they have no competing financial interests.

Acknowledgments

The authors thank Sabine Vidal-y-Sy, Ewa Wladykowski and Mona Grønning for excellent technical assistance. We thank also Dr. Antonio Virgilio Failla of the Microscopy Imaging Facility, University Medical Center Hamburg-Eppendorf, to support our STED microscopic analysis.

Supplementary materials

Supplementary material associated with this article can be found, in the online version, at doi:10.1016/j.matbio.2022.06.002.

Received 13 January 2022;
Received in revised form 28 April 2022;
Accepted 7 June 2022
Available online 9 June 2022

Keywords:
Heparan sulfate;
Melanoma;
von Willebrand factor;
Circulating tumor cells;
Metastasis

Abbreviations:
vWF, von Willebrand factor; HS, Heparan sulfate; ULvWF, Ultra-large vWF; CTCs, Circulating tumour cells; SDC, Syndecan; EXT1, Exostosin 1; EXT2, Exostosin 2; NDST, Glucosaminyl N-deacetylase/N-sulfotransferase; HA, Hyaluronic acid; CS, Chondroitin sulfate; WGA, Wheat germ agglutinin; STED, Stimulated emission depletion; ECIS, Electric cell-impedance sensing; RICM, Reflection interference contrast microscopy; VCAM1, Vascular cell adhesion protein 1; VLA4, Very late antigen 4; SMFS, Single molecular force spectroscopy; AFM, Atomic force microscopy; SAW, Surface acoustic wave; ADAMTS13, A disintegrin−like and metalloproteinase with thrombospondin type 1 motif 13; HUVECs, Human umbilical vein endothelial cells; HPSE, Heparanase; HAS, Hyaluronan Synthase; HYAL, Hyaluronidase; CHSY, Chondroitin sulfate synthase; CHPF, Chondroitin sulfate synthase 2

[1]These authors contributed equally to this work.

References

[1] J.R. Bishop, M. Schuksz, J.D. Esko, Heparan sulphate proteoglycans fine-tune mammalian physiology, Nature 446 (7139) (2007) 1030–1037.
[2] S. Sarrazin, W.C. Lamanna, J.D. Esko, Heparan sulfate proteoglycans, Cold Spring Harb. Perspect. Biol. 3 (7) (2011) 1–33.
[3] J.P. Li, M. Kusche-Gullberg, K.W. Jeon, Chapter six - heparan sulfate: biosynthesis, structure, and function, International Review of Cell and Molecular Biology, Academic Press, 2016, pp. 215–273.
[4] N. Hassan, B. Greve, N.A. Espinoza-Sánchez, M. Götte, Cell-surface heparan sulfate proteoglycans as multifunctional integrators of signaling in cancer, Cell. Signal. 77 (2021) 109822.
[5] K. Raman, B. Kuberan, Chemical tumor biology of heparan sulfate proteoglycans, Curr. Chem. Biol. 4 (1) (2010) 20–31.
[6] R.D. Sanderson, S.K. Bandari, I. Vlodavsky, Proteases and glycosidases on the surface of exosomes: newly discovered mechanisms for extracellular remodeling, Matrix Biol. 75-76 (2019) 160–169.
[7] O. Vornicova, I. Boyango, S. Feld, I. Naroditsky, O. Kazarin, Y. Zohar, Y. Tiram, N. Ilan, O. Ben-Izhak, I. Vlodavsky, G. Bar-Sela, The prognostic significance of heparanase expression in metastatic melanoma, Oncotarget 7 (46) (2016) 74678–74685.
[8] L. von Palubitzki, Y. Wang, S. Hoffmann, Y.S.S. Vidal, B. Zobiak, A.V. Failla, P. Schmage, A. John, A. Osorio-Madrazo, A.T. Bauer, S.W. Schneider, F.M. Goycoolea, C. Gorzelanny, Differences of the tumour cell glycocalyx affect binding of capsaicin-loaded chitosan nanocapsules, Sci. Rep. 10 (1) (2020) 22443.
[9] V. Vanheule, D. Boff, A. Mortier, R. Janssens, B. Petri, E. Kolaczkowska, P. Kubes, N. Berghmans, S. Struyf, A.J. Kungl, M.M. Teixeira, F.A. Amaral, P. Proost, CXCL9-derived peptides differentially inhibit neutrophil migration *in vivo* through interference with glycosaminoglycan interactions, Front. Immunol. 8 (2017) 530.
[10] F. Peysselon, S. Ricard-Blum, Heparin-protein interactions: from affinity and kinetics to biological roles. Application to an interaction network regulating angiogenesis, Matrix Biol. 35 (2014) 73–81.
[11] M. Schlesinger, D. Simonis, P. Schmitz, J. Fritzsche, G. Bendas, Binding between heparin and the integrin VLA-4, Thromb. Haemost. 102 (5) (2009) 816–822.
[12] M.J. Paszek, C.C. DuFort, O. Rossier, R. Bainer, J.K. Mouw, K. Godula, J.E. Hudak, J.N. Lakins, A.C. Wijekoon, L. Cassereau, M.G. Rubashkin, M.J. Magbanua, K.S. Thorn, M.W. Davidson, H.S. Rugo, J.W. Park, D.A. Hammer, G. Giannone, C.R. Bertozzi, V.M. Weaver, The cancer glycocalyx mechanically primes integrin-mediated growth and survival, Nature 511 (7509) (2014) 319–325.
[13] K. Arnold, Y. Xu, Y.E. Liao, B.C. Cooley, R. Pawlinski, J. Liu, Synthetic anticoagulant heparan sulfate attenuates liver ischemia reperfusion injury, Sci. Rep. 10 (1) (2020) 17187.
[14] T. Kalagara, T. Moutsis, Y. Yang, K.I. Pappelbaum, A. Farken, L. Cladder-Micus, Y.S.S. Vidal, A. John, A.T. Bauer, B.M. Moerschbacher, S.W. Schneider, C. Gorzelanny, The endothelial glycocalyx anchors von Willebrand factor fibers to the vascular endothelium, Blood Adv. 2 (18) (2018) 2347–2357.
[15] J. Huang, R. Roth, J.E. Heuser, J.E. Sadler, Integrin alpha(v) beta(3) on human endothelial cells binds von Willebrand factor strings under fluid shear stress, Blood 113 (7) (2009) 1589–1597.
[16] J.M. O'Sullivan, R.J. Preston, N. O'Regan, J.S. O'Donnell, Emerging roles for hemostatic dysfunction in malaria pathogenesis, Blood 127 (19) (2016) 2281–2288.
[17] C.Y. Goh, S. Patmore, A. Smolenski, J. Howard, S. Evans, J. O'Sullivan, A. McCann, The role of von Willebrand factor

in breast cancer metastasis, Transl. Oncol. 14 (4) (2021) 101033.
[18] E.S. Hatzipantelis, M. Athanassiou-Metaxa, N. Gombakis, V. Tzimouli, A. Taparkou, V. Sidi-Fragandrea, V. Garipidou, T. Papageorgiou, D. Kleta, D.E. Koliouskas, F. Athanasiadou-Piperopoulou, Thrombomodulin and von Willebrand factor: relation to endothelial dysfunction and disease outcome in children with acute lymphoblastic leukemia, Acta Haematol. 125 (3) (2011) 130–135.
[19] V.S. Schellerer, L. Mueller-Bergh, S. Merkel, R. Zimmermann, D. Weiss, A. Schlabrakowski, E. Naschberger, M. Stürzl, W. Hohenberger, R.S. Croner, The clinical value of von Willebrand factor in colorectal carcinomas, Am. J. Transl. Res. 3 (5) (2011) 445–453.
[20] W.S. Wang, J.K. Lin, T.C. Lin, T.J. Chiou, J.H. Liu, C.C. Yen, P.M. Chen, Plasma von Willebrand factor level as a prognostic indicator of patients with metastatic colorectal carcinoma, World J. Gastroenterol. 11 (14) (2005) 2166–2170.
[21] Z. Zietek, I. Iwan-Zietek, R. Paczulski, M. Kotschy, Z. Wolski, von Willebrand factor antigen in blood plasma of patients with urinary bladder carcinoma, Thromb. Res. 83 (5) (1996) 399–402.
[22] C. Schwarz, F. Fitschek, M. Mittlböck, V. Saukel, S. Bota, M. Ferlitsch, A. Ferlitsch, M. Bodingbauer, K. Kaczirek, von Willebrand factor antigen predicts outcomes in patients after liver resection of hepatocellular carcinoma, Gut Liver 14 (2) (2020) 218–224.
[23] H.L. Obermeier, J. Riedl, C. Ay, S. Koder, P. Quehenberger, R. Bartsch, A. Kaider, C.C. Zielinski, I. Pabinger, The role of ADAMTS-13 and von Willebrand factor in cancer patients: results from the Vienna cancer and thrombosis study, Res. Pract. Thromb. Haemost. 3 (3) (2019) 503–514.
[24] A.T. Bauer, J. Suckau, K. Frank, A. Desch, L. Goertz, A.H. Wagner, M. Hecker, T. Goerge, L. Umansky, P. Beckhove, J. Utikal, C. Gorzelanny, N. Diaz-Valdes, V. Umansky, S.W. Schneider, von Willebrand factor fibers promote cancer-associated platelet aggregation in malignant melanoma of mice and humans, Blood 125 (20) (2015) 3153–3163.
[25] C.M. Suter, P.J. Hogg, J.T. Price, B.H. Chong, R.L. Ward, Identification and characterisation of a platelet GPIb/V/IX-like complex on human breast cancers: implications for the metastatic process, Jpn. J. Cancer Res. 92 (10) (2001) 1082–1092.
[26] V. Terraube, R. Pendu, D. Baruch, M.F. Gebbink, D. Meyer, P.J. Lenting, C.V. Denis, Increased metastatic potential of tumor cells in von Willebrand factor-deficient mice, J. Thromb. Haemost. 4 (3) (2006) 519–526.
[27] L. Goertz, S.W. Schneider, A. Desch, F.T. Mayer, J. Koett, K. Nowak, I. Karampinis, M.K. Bohlmann, V. Umansky, A.T. Bauer, Heparins that block VEGF-A-mediated von Willebrand factor fiber generation are potent inhibitors of hematogenous but not lymphatic metastasis, Oncotarget 7 (42) (2016) 68527–68545.
[28] D. Schadendorf, A.C.J. van Akkooi, C. Berking, K.G. Griewank, R. Gutzmer, A. Hauschild, A. Stang, A. Roesch, S. Ugurel, Melanoma, Lancet 392 (10151) (2018) 971–984.
[29] L. Chen, A.M. Bode, Z. Dong, Circulating tumor cells: moving biological insights into detection, Theranostics 7 (10) (2017) 2606–2619.
[30] R. Leblanc, O. Peyruchaud, Metastasis: new functional implications of platelets and megakaryocytes, Blood 128 (1) (2016) 24–31.
[31] M.P. Ward, L.E. Kane, L.A. Norris, B.M. Mohamed, T. Kelly, M. Bates, A. Clarke, N. Brady, C.M. Martin, R.D. Brooks, D.A. Brooks, S. Selemidis, S. Hanniffy, E.P. Dixon, S.A. O'Toole, J.J. O'Leary, Platelets, immune cells and the coagulation cascade; friend or foe of the circulating tumour cell? Mol. Cancer 20 (1) (2021) 59.
[32] P.A. Burke, S.J. DeNardo, L.A. Miers, K.R. Lamborn, S. Matzku, G.L. DeNardo, Cilengitide targeting of $\alpha_v\beta_3$integrin receptor synergizes with radioimmunotherapy to increase efficacy and apoptosis in breast cancer xenografts, Cancer Res. 62 (15) (2002) 4263–4272.
[33] M. Busse, A. Feta, J. Presto, M. Wilén, M. Grønning, L. Kjellén, M. Kusche-Gullberg, Contribution of EXT1, EXT2, and EXTL3 to heparan sulfate chain elongation, J. Biol. Chem. 282 (45) (2007) 32802–32810.
[34] J. Presto, M. Thuveson, P. Carlsson, M. Busse, M. Wilén, I. Eriksson, M. Kusche-Gullberg, L. Kjellén, Heparan sulfate biosynthesis enzymes EXT1 and EXT2 affect NDST1 expression and heparan sulfate sulfation, Proc. Natl. Acad. Sci. U. S. A 105 (12) (2008) 4751–4756.
[35] G. Pavlov, S. Finet, K. Tatarenko, E. Korneeva, C. Ebel, Conformation of heparin studied with macromolecular hydrodynamic methods and X-ray scattering, Eur. Biophys. J. EBJ 32 (5) (2003) 437–449.
[36] E. Cerami, J. Gao, U. Dogrusoz, B.E. Gross, S.O. Sumer, B.A. Aksoy, A. Jacobsen, C.J. Byrne, M.L. Heuer, E. Larsson, Y. Antipin, B. Reva, A.P. Goldberg, C. Sander, N. Schultz, The cBio cancer genomics portal: an open platform for exploring multidimensional cancer genomics data, Cancer Discov. 2 (5) (2012) 401–404.
[37] J. Gao, B.A. Aksoy, U. Dogrusoz, G. Dresdner, B. Gross, S.O. Sumer, Y. Sun, A. Jacobsen, R. Sinha, E. Larsson, E. Cerami, C. Sander, N. Schultz, Integrative analysis of complex cancer genomics and clinical profiles using the cBioPortal, Sci. Signal. 6 (269) (2013) pl1.
[38] C. Koch, A. Kuske, S.A. Joosse, G. Yigit, G. Sflomos, S. Thaler, D.J. Smit, S. Werner, K. Borgmann, S. Gartner, P. Mossahebi Mohammadi, L. Battista, L. Cayrefourcq, J. Altmuller, G. Salinas-Riester, K. Raithatha, A. Zibat, Y. Goy, L. Ott, K. Bartkowiak, T.Z. Tan, Q. Zhou, M.R. Speicher, V. Muller, T.M. Gorges, M. Jucker, J.P. Thiery, C. Brisken, S. Riethdorf, C. Alix-Panabieres, K. Pantel, Characterization of circulating breast cancer cells with tumorigenic and metastatic capacity, EMBO Mol. Med. 12 (9) (2020) e11908.
[39] L.M. Gockel, M. Heyes, H. Li, A. Al Nahain, C. Gorzelanny, M. Schlesinger, S. Holdenrieder, J.P. Li, V. Ferro, G. Bendas, Inhibition of tumor-host cell interactions using synthetic heparin mimetics, ACS Appl. Mater. Interfaces 13 (6) (2021) 7080–7093.
[40] F. Burgos-Bravo, S. Martínez-Meza, A.F.G. Quest, C.A.M. Wilson, L. Leyton, Application of force to a syndecan-4 containing complex with Thy-1-α(V)β(3) integrin accelerates neurite retraction, Front. Mol. Biosci. 7 (2020) 582257.
[41] S. Starzonek, H. Maar, V. Labitzky, D. Wicklein, C. Rossdam, F.F.R. Buettner, G. Wolters-Eisfeld, C. Guengoer, C. Wagener, U. Schumacher, T. Lange, Systematic analysis of the human tumor cell binding to human vs. murine E- and P-selectin under static vs. dynamic conditions, Glycobiology 30 (9) (2020) 695–709.
[42] M. Schlesinger, M. Roblek, K. Ortmann, A. Naggi, G. Torri, L. Borsig, G. Bendas, The role of VLA-4 binding for experimental melanoma metastasis and its inhibition by heparin, Thromb. Res. 133 (5) (2014) 855–862.

[43] I. Singh, H. Shankaran, M.E. Beauharnois, Z. Xiao, P. Alexandridis, S. Neelamegham, Solution structure of human von Willebrand factor studied using small angle neutron scattering, J. Biol. Chem. 281 (50) (2006) 38266–38275.
[44] X. Zhang, S.E. Craig, H. Kirby, M.J. Humphries, V.T. Moy, Molecular basis for the dynamic strength of the integrin alpha4beta1/VCAM-1 interaction, Biophys. J. 87 (5) (2004) 3470–3478.
[45] Y. Yang, C. Gorzelanny, A.T. Bauer, N. Halter, D. Komljenovic, T. Bäuerle, L. Borsig, M. Roblek, S.W. Schneider, Nuclear heparanase-1 activity suppresses melanoma progression via its DNA-binding affinity, Oncogene 34 (47) (2015) 5832–5842.
[46] N.J. Nasser, A. Avivi, I. Shafat, E. Edovitsky, E. Zcharia, N. Ilan, I. Vlodavsky, E. Nevo, Alternatively spliced Spalax heparanase inhibits extracellular matrix degradation, tumor growth, and metastasis, Proc. Natl. Acad. Sci. U. S. A. 106 (7) (2009) 2253–2258.
[47] M. Hoore, K. Rack, D.A. Fedosov, G. Gompper, Flow-induced adhesion of shear-activated polymers to a substrate, J. Phys. Condens. Matter 30 (6) (2018) 064001 An Institute of Physics Journal.
[48] M.J. Feinauer, S.W. Schneider, A.S. Berghoff, J.R. Robador, C. Tehranian, M.A. Karreman, V. Venkataramani, G. Solecki, J.K. Grosch, K. Gunkel, B. Kovalchuk, F.T. Mayer, M. Fischer, M.O. Breckwoldt, M. Brune, Y. Schwab, W. Wick, A.T. Bauer, F. Winkler, Local blood coagulation drives cancer cell arrest and brain metastasis in a mouse model, Blood 137 (9) (2021) 1219–1232.
[49] H.L. Obermeier, J. Riedl, C. Ay, S. Koder, P. Quehenberger, R. Bartsch, A. Kaider, C.C. Zielinski, I. Pabinger, The role of ADAMTS-13 and von Willebrand factor in cancer patients: results from the Vienna cancer and thrombosis study, Res. Pract. Thromb. Haemost. 3 (3) (2019) 503–514.
[50] A. Abramsson, S. Kurup, M. Busse, S. Yamada, P. Lindblom, E. Schallmeiner, D. Stenzel, D. Sauvaget, J. Ledin, M. Ringvall, U. Landegren, L. Kjellén, G. Bondjers, J.P. Li, U. Lindahl, D. Spillmann, C. Betsholtz, H. Gerhardt, Defective N-sulfation of heparan sulfate proteoglycans limits PDGF-BB binding and pericyte recruitment in vascular development, Genes Dev. 21 (3) (2007) 316–331.
[51] V.F. Fiore, L. Ju, Y. Chen, C. Zhu, T.H. Barker, Dynamic catch of a Thy-1-alpha5beta1+syndecan-4 trimolecular complex, Nat. Commun. 5 (2014) 4886.
[52] D.M. Beauvais, B.J. Burbach, A.C. Rapraeger, The syndecan-1 ectodomain regulates alphavbeta3 integrin activity in human mammary carcinoma cells, J. Cell Biol. 167 (1) (2004) 171–181.
[53] B. Mulloy, The specificity of interactions between proteins and sulfated polysaccharides, An. Acad. Bras. Cienc. 77 (4) (2005) 651–664.
[54] V. Huck, M.F. Schneider, C. Gorzelanny, S.W. Schneider, The various states of von Willebrand factor and their function in physiology and pathophysiology, Thromb. Haemost. 111 (4) (2014) 598–609.
[55] C. Bret, D. Hose, T. Reme, A.C. Sprynski, K. Mahtouk, J.F. Schved, P. Quittet, J.F. Rossi, H. Goldschmidt, B. Klein, Expression of genes encoding for proteins involved in heparan sulphate and chondroitin sulphate chain synthesis and modification in normal and malignant plasma cells, Br. J. Haematol. 145 (3) (2009) 350–368.
[56] L.E. Collins, L. Troeberg, Heparan sulfate as a regulator of inflammation and immunity, J. Leukoc. Biol. 105 (1) (2019) 81–92.
[57] P. Martinez, A. Denys, M. Delos, A.S. Sikora, M. Carpentier, S. Julien, J. Pestel, F. Allain, Macrophage polarization alters the expression and sulfation pattern of glycosaminoglycans, Glycobiology 25 (5) (2015) 502–513.
[58] O.A. Martin, R.L. Anderson, K. Narayan, M.P. MacManus, Does the mobilization of circulating tumour cells during cancer therapy cause metastasis? Nat. Rev. Clin. Oncol. 14 (1) (2017) 32–44.
[59] S.A. Joosse, B. Beyer, C. Gasch, P. Nastały, A. Kuske, H. Isbarn, L.J. Horst, C. Hille, T.M. Gorges, L. Cayrefourcq, C. Alix-Panabières, P. Tennstedt, S. Riethdorf, T. Schlomm, K. Pantel, Tumor-associated release of prostatic cells into the blood after transrectal ultrasound-guided biopsy in patients with histologically confirmed prostate cancer, Clin. Chem. 66 (1) (2019) 161–168.
[60] K.A. Hoadley, C. Yau, T. Hinoue, D.M. Wolf, A.J. Lazar, E. Drill, R. Shen, A.M. Taylor, A.D. Cherniack, V. Thorsson, R. Akbani, R. Bowlby, C.K. Wong, M. Wiznerowicz, F. Sanchez-Vega, A.G. Robertson, B.G. Schneider, M.S. Lawrence, H. Noushmehr, T.M. Malta, J.M. Stuart, C.C. Benz, P.W. Laird, Cell-of-origin patterns dominate the molecular classification of 10,000 tumors from 33 types of cancer, Cell 173 (2) (2018) 291–304.e6.
[61] E. Cerami, J. Gao, U. Dogrusoz, B.E. Gross, S.O. Sumer, B.A. Aksoy, A. Jacobsen, C.J. Byrne, M.L. Heuer, E. Larsson, Y. Antipin, B. Reva, A.P. Goldberg, C. Sander, N. Schultz, The cBio cancer genomics portal: an open platform for exploring multidimensional cancer genomics data, Cancer Discov. 2 (5) (2012) 401–404.
[62] U. Richter, C. Schröder, D. Wicklein, T. Lange, S. Geleff, V. Dippel, U. Schumacher, S. Klutmann, Adhesion of small cell lung cancer cells to E- and P-selectin under physiological flow conditions: implications for metastasis formation, Histochem. Cell Biol. 135 (5) (2011) 499–512.
[63] C. Gorzelanny, B. Poppelmann, K. Pappelbaum, B.M. Moerschbacher, S.W. Schneider, Human macrophage activation triggered by chitotriosidase-mediated chitin and chitosan degradation, Biomaterials 31 (33) (2010) 8556–8563.
[64] L.M. Gockel, M. Heyes, H. Li, A. Al Nahain, C. Gorzelanny, M. Schlesinger, S. Holdenrieder, J.P. Li, V. Ferro, G. Bendas, Inhibition of tumor−host cell interactions using synthetic heparin mimetics, ACS Appl. Mater. Interfaces 13 (6) (2021) 7080–7093.
[65] J.E. Shively, H.E. Conrad, Formation of anhydrosugars in the chemical depolymerization of heparin, Biochemistry 15 (18) (1976) 3932–3942.
[66] I. Giaever, C.R. Keese, Micromotion of mammalian cells measured electrically, Proc. Natl. Acad. Sci. 88 (17) (1991) 7896.
[67] T.D. Becke, S. Ness, S. Sudhop, H.E. Gaub, M. Hilleringmann, A.F. Schilling, H. Clausen-Schaumann, Covalent immobilization of proteins for the single molecule force spectroscopy, J. Vis. Exp. JoVE (138) (2018) 1–10.
[68] R. Merkel, P. Nassoy, A. Leung, K. Ritchie, E. Evans, Energy landscapes of receptor-ligand bonds explored with dynamic force spectroscopy, Nature 397 (6714) (1999) 50–53.
[69] D.C. Lin, F. Horkay, Nanomechanics of polymer gels and biological tissues: a critical review of analytical approaches in the hertzian regime and beyond, Soft Matter 4 (4) (2008) 669–682.
[70] C.A. Schneider, W.S. Rasband, K.W. Eliceiri, NIH image to ImageJ: 25 years of image analysis, Nat. Methods 9 (7) (2012) 671–675.
[71] F.A. Ran, P.D. Hsu, J. Wright, V. Agarwala, D.A. Scott, F. Zhang, Genome engineering using the CRISPR-Cas9 system, Nat. Protoc. 8 (11) (2013) 2281–2308.